

Active arc-continent collision: Earthquakes, gravity anomalies, and fault kinematics in the Huon-Finisterre collision zone, Papua New Guinea

Geoffrey A. Abers

Lamont-Doherty Earth Observatory of Columbia University, Palisades, New York

Robert McCaffrey

Rensselaer Polytechnic Institute, Troy, New York

Abstract. The Huon-Finisterre island arc terrane is actively colliding with the north edge of the Australian continent. The collision provides a rare opportunity to study continental accretion while it occurs. We examine the geometry and kinematics of the collision by comparing earthquake source parameters to surface fault geometries and plate motions, and we constrain the forces active in the collision by comparing topographic loads to gravity anomalies. Waveform inversion is used to constrain focal mechanisms for 21 shallow earthquakes that occurred between 1966 and 1992 (seismic moment 10^{17} to 3×10^{20} N m). Twelve earthquakes show thrust faulting at 22-37 km depth. The largest thrust events are on the north side of the Huon Peninsula and are consistent with slip on the Ramu-Markham thrust fault zone, the northeast dipping thrust fault system that bounds the Huon-Finisterre terrane. Thus much of the terrane's crust but little of its mantle is presently being added to the Australian continent. The large thrust earthquakes also reveal a plausible mechanism for the uplift of Pleistocene coral terraces on the north side of the Huon Peninsula. Bouguer gravity anomalies are too negative to allow simple regional compensation of topography and require large additional downward forces to depress the lower plate beneath the Huon Peninsula. With such forces, plate configurations are found that are consistent with observed gravity and basin geometry. Other earthquakes give evidence of deformation above and below the Ramu-Markham thrust system. Four thrust events, 22-27 km depth directly below the Ramu-Markham fault outcrop, are too deep to be part of a planar Ramu-Markham thrust system and may connect to the north dipping Highlands thrust system farther south. Two large strike-slip faulting earthquakes and their aftershocks, in 1970 and 1987, show faulting within the upper plate of the thrust system. The inferred fault planes show slip vectors parallel to those on nearby thrust faults, and may represent small offsets in the overriding plate. These faults, along with small normal-faulting earthquakes beneath the Huon-Finisterre ranges and a 25° along-strike rotation of slip vectors, demonstrate the presence of along-strike extension of the accreting terrane and along-strike compression of the lower plate.

Introduction

The Neogene orogenic belt on the island of New Guinea is the consequence of collision between an island arc and the northern margin of the Australian continent [Dewey and Bird, 1970; Hamilton, 1979]. Although seismicity catalogs suggest that the orogenic belt is now a diffuse zone of deformation [e.g., Johnson and Molnar, 1972; Cullen and Pigott, 1989], many active boundaries are localized rather than diffuse, and localized motion on major fault zones may be the predominant mode of deformation. Because New Guinea is one of the few active examples of arc-continent collision, the deformation patterns occurring in New Guinea provide evidence for processes that emplaced older accreted terranes elsewhere.

Although some of Australia-Pacific convergence is accommodated by building mountains from the former Australian margin in the New Guinea Highlands [e.g., Abers and McCaffrey, 1988], most seismicity and most evidence for Quaternary uplift is associated with the arc-continent collision in northern New Guinea, the Huon-Finisterre (HF) collision [e.g., Chappell, 1974; Cooper and Taylor, 1987]. The aim of this paper is to elucidate the regional patterns and rates of active faulting in the HF collision zone of eastern New Guinea. Focal mechanisms and depths of earthquakes, gravity, and other geologic data, are used to study an island arc terrane that has recently collided with a continent. Our results show that strike-slip faulting within the arc terrane is significant, suggesting that the island arc terrane is rapidly being dismembered. Thrust-faulting earthquakes thought to indicate terrane emplacement extend to 30-40 km depths, and show that much or all of the crust of the former island arc is accreting to the continent.

Regional Tectonics

The major structures in New Guinea strike E-W to NW-SE (Figure 1) although in this area the Pacific and Australian plates are converging at an azimuth of near 70° [DeMets *et al.*, 1990]. Several subparallel structures partition slip in a wide zone between major plates. In eastern New Guinea most of the E-W motion is taken up by transform faulting in the Bismarck Sea [Taylor, 1979], so the expected convergence direction east of 145° E is nearly N-S, perpendicular to regional structures. Onshore structures in eastern New Guinea are predominantly compressional [e.g., Rogerson *et al.*, 1988] although many

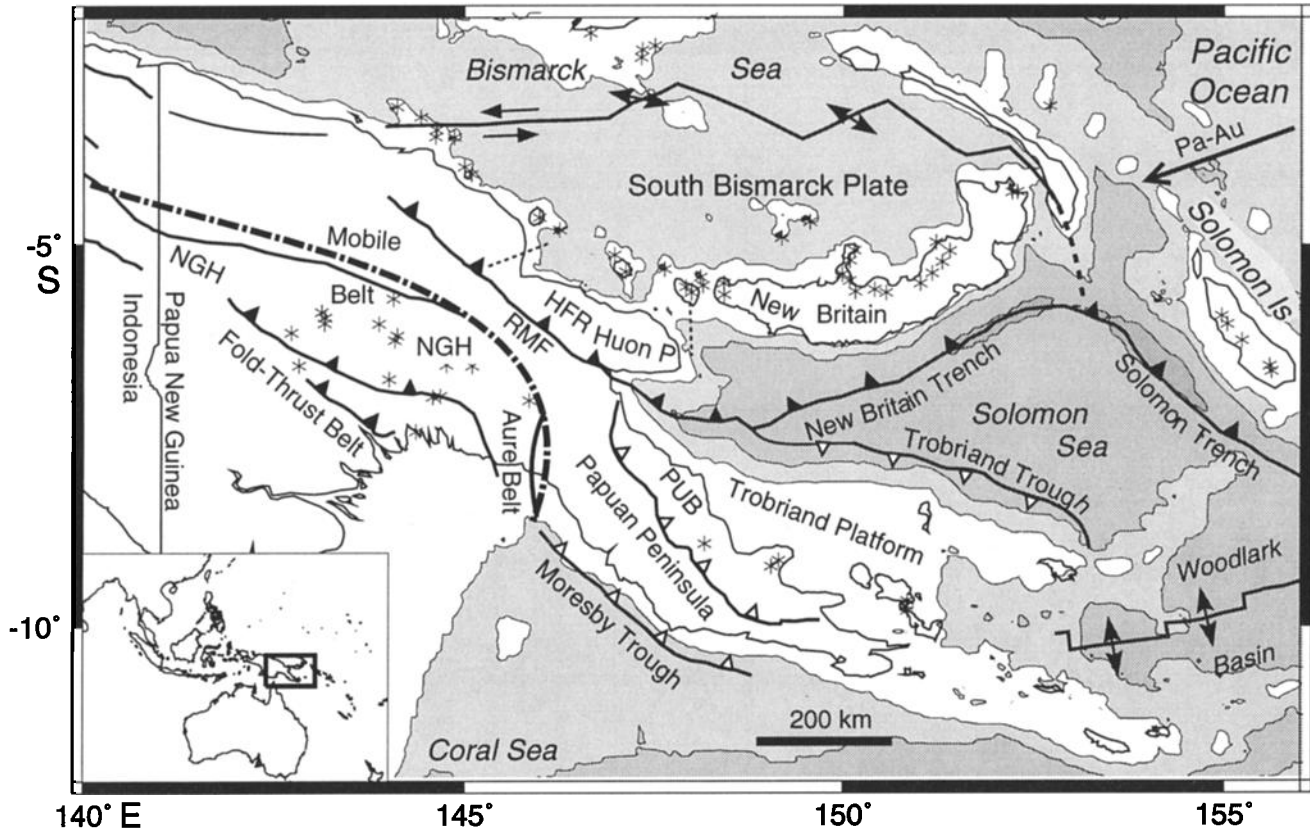


Figure 1. The Papua New Guinea region. Star symbols denote Quaternary volcanic centers; thick solid lines show major faults [D'Addario *et al.*, 1976], thin dashed lines show inferred strike-slip faults, and the thick dot-dashed line shows approximate northern limit of exposed Australian continental basement [Hamilton, 1979]. Fault slip is indicated by arrows and by triangles on the hanging walls of thrust faults (open triangles where present motion is slow or inactive). Bathymetry, denoted by shading, is contoured at 1000 m, 3000 m, and 7000 m depths. Key: Pa-Au, direction of Pacific-Australia relative motion [DeMets *et al.*, 1990]; HFR, Huon-Finisterre Ranges; Huon P, Huon Peninsula; NGH, New Guinea Highlands; PUB, Papuan ultramafic belt; and RMF, Ramu-Markham fault.

structures have been interpreted as the result of left-lateral shear [e.g., Krause, 1965; Cullen and Pigott, 1989]. Convergence is accommodated in two major north dipping thrust systems, the Ramu-Markham (RM) fault zone that forms the southern boundary of the Finisterre-Huon island arc terrane [e.g., Silver *et al.*, 1991] and the New Guinea Highlands thrust belt composed of the former passive Australian margin [e.g., Jenkins, 1974]. Seismicity in eastern New Guinea is concentrated near and north of the terrane-bounding faults [e.g., Cooper and Taylor, 1987; Abers and Roecker, 1991]. Hence most of the convergence takes place there, although some earthquakes occur in the Highlands thrust belt [Abers and McCaffrey, 1988].

The main phase of the present arc-continent collision in New Guinea began in late Miocene time [Dow, 1977], and deformation has continued throughout the orogen for at least the last 3-5 Ma. The northern edge of the Australian craton [e.g., Dow, 1977; Hamilton, 1979] underlies a foreland basin, in southern New Guinea, and extends north at least beneath a south vergent thrust belt. The thrust belt of deformed continental margin sediments forms the New Guinea Highlands. Metamorphic rocks and scattered ophiolites flank the northern

margins of the ranges [e.g., Dow, 1977]. Continental basement rocks are found throughout much of the Highlands and occasionally farther north, evidence that much of the island is underlain by continental crust [Rogerson *et al.*, 1988]. The Ramu-Markham (RM) Valley in eastern New Guinea separates rocks of continental affinity from the accreting island arc terrane and contains several kilometers of Neogene sediments.

In eastern New Guinea the 2-4 km high Finisterre-Huon (FH) ranges follow the north coast, an accreting island arc terrane [Davies *et al.*, 1987; Silver *et al.*, 1991]. The onset of the FH collision has been dated at ~3-4 Ma, for example by a transition from quartz- and schist-rich to volcanolithic turbidites in the collision zone [Abbott and Silver, 1991], although some workers prefer mid-Miocene dates (H. Davies, personal communication, 1993). The collision is generally younger in the east than in the west. The active suture, the RM fault zone, continues east along strike to the New Britain Trench, where arc-continent collision has not yet occurred. A Wadati-Benioff zone still exists beneath the HF terrane at 100-250 km depth, continuous along strike with the New Britain Wadati-Benioff zone below 125 km depth but not in the upper 100 km [Abers and Roecker, 1991].

Waveform Inversion

Method

We use a teleseismic body wave inversion technique [Nábělek, 1984] to determine source parameters for 21 shallow earthquakes in eastern New Guinea (Table 1, Figures 2 and 3). Solutions for 18 additional events from the Highlands thrust belt have been discussed previously [Abers and McCaffrey, 1988] as have a number of events in central and western New Guinea north of the Highlands [Abers, 1989; McCaffrey and Abers, 1991]. All events in the region were examined with International Seismological Centre (ISC) catalog depths above 85 km, and results are presented for those with sufficient available waveforms and with depths less than 75 km from inversion. Hence the earthquakes discussed here are a complete set of solutions for shallow events (depth < 50-75 km) in the HF region between 1963 and 1992.

Seismograms were taken from analog (WWSSN) and digital global networks for stations at epicentral distances of 30°-90° for long period *P* waves, or 30°-70° for long-period *SH* waves. Digital broadband displacement records were obtained by directly deconvolving instrument response from records of broadband channels or by combining the digital long-period and short-period waveforms [Harvey and Choy, 1982]. The deconvolutions were stabilized using filters with a passband from 0.01-0.02 to 1.0 Hz, although occasionally narrower ranges were used to remove long-period or microseismic noise. Arrival times were set to the times of observed arrivals on short-period records, when available.

Table 1. Relocated Epicenters for Earthquakes Studied

Date	Origin Time, UTC	Latitude, °S	Longitude, °E	<i>m</i> <i>b</i> *
1966/12/23	1550:21.3	6.88	148.34	6.1
1967/ 9/18	1533:06.6	5.80	146.76	5.6
1970/10/31	1753:08.9	4.96	145.83	6.0
1970/11/12	0607:15.4	5.03	145.21	6.2
1972/ 1/18	2155:16.5	4.96	145.00	5.8
1972/ 1/19	1500:51.3	4.56	145.04	5.9
1980/ 6/25	1848:11.8	6.66	147.15	5.6
1982/ 9/14	1817:06.8	7.30	148.09	5.3
1983/ 3/11	0310:42.7	6.97	147.62	5.9
1986/ 2/12a	0901:09.9	6.62	147.49	5.7
1986/ 2/12b	1127:46.1	6.62	147.47	5.5
1987/ 2/ 7	1157:34.0	5.72	147.93	5.5
1987/ 2/ 8	1833:59.1	5.87	147.91	6.1
1987/ 2/ 9	1817:31.0	5.94	147.93	5.6
1987/ 2/25	1127:10.7	6.05	147.89	5.7
1987/ 3/16	1549:38.5	6.41	147.78	5.6
1992/ 2/21†	1442:28.9	6.24	147.67	5.5
1992/ 2/27†	2005:27.2	6.22	147.62	5.8
1992/ 5/15†	0705:04.7	6.06	147.59	6.2
1992/ 5/21†	1409:03.1	6.20	147.32	5.6
1992/12/18†	0314:04.9	6.51	147.22	6.0

*Body wave magnitude from International Seismological Centre catalog for events before 1990 and National Earthquake Information Center PDE catalog otherwise.

†Not relocated; NEIC epicenter used.

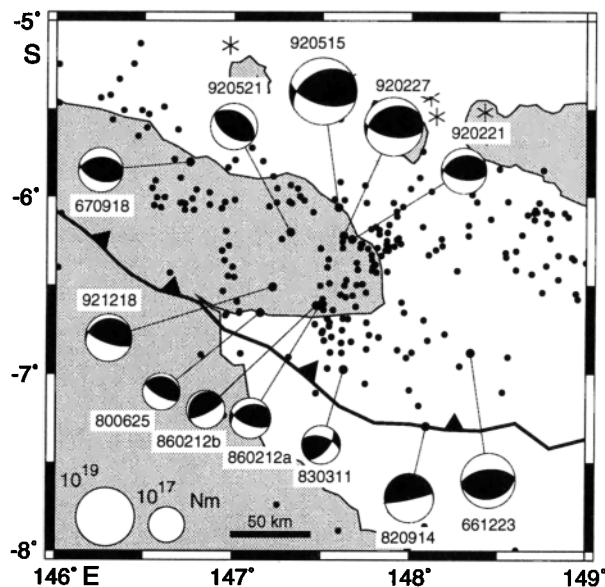


Figure 2. Fault-plane solutions for thrust events in the Huon region (Table 2). Solutions plotted as lower hemisphere equal-area projections, with radius proportional to log of seismic moment, scale lower left. Dots show relocated earthquakes with depths less than 70 km, from Abers and Roecker [1991]. Events occurring in 1992 were not relocated; instead, NEIC epicenters were used. Barbed line shows surface trace of Ramu-Markham fault and its eastward extension, the New Britain trench. Star symbols show Quaternary volcanos.

The inversion determines the strike and dip of one fault plane and the rake of the slip vector (using the convention of Aki and Richards [1980]), the source depth, the seismic moment M_0 , and the shape of the source time function parameterized by a series of overlapping isosceles triangles (Table 2) [Nábělek, 1985]. Duration (t_{95}) is determined from the source-time function, as the 95% width (± 2 standard deviations) about the centroid. Other details of processing and inversion are discussed by Nábělek [1984] and McCaffrey et al. [1991].

A half-space source structure was assumed with *P* velocity V_P of 6.5 km s⁻¹, *S* velocity V_S of 3.7 km s⁻¹ and density ρ of 2800 kg m⁻³, with a few exceptions. These values are consistent with velocities determined for crust in the HF region [Abers and Roecker, 1991]. Events 661223, 820914, and 830311 are beneath the Huon Gulf, so the source structure included a water layer 3, 4, and 2.5 km deep, respectively, based on water depths at the epicenter. Although these depths may be somewhat in error, departures from plane-layered structure could produce comparable errors. Events 800625, 860212a, 860212b, and 921218 were all near the southern flank of the HF ranges or beneath the RM Valley. For these events, pronounced "W"-shaped *P* wave pulses were observed, suggesting reverberation within a sedimentary layer above the source, so a 5-km-thick top layer representing sediments was included in the source region structure, with $V_P = 4.5$ km s⁻¹, $V_S = 2.6$ km s⁻¹, and $\rho = 2400$ kg m⁻³. This basin thickness and density are consistent with the gravity observations across the basin margin, discussed below.

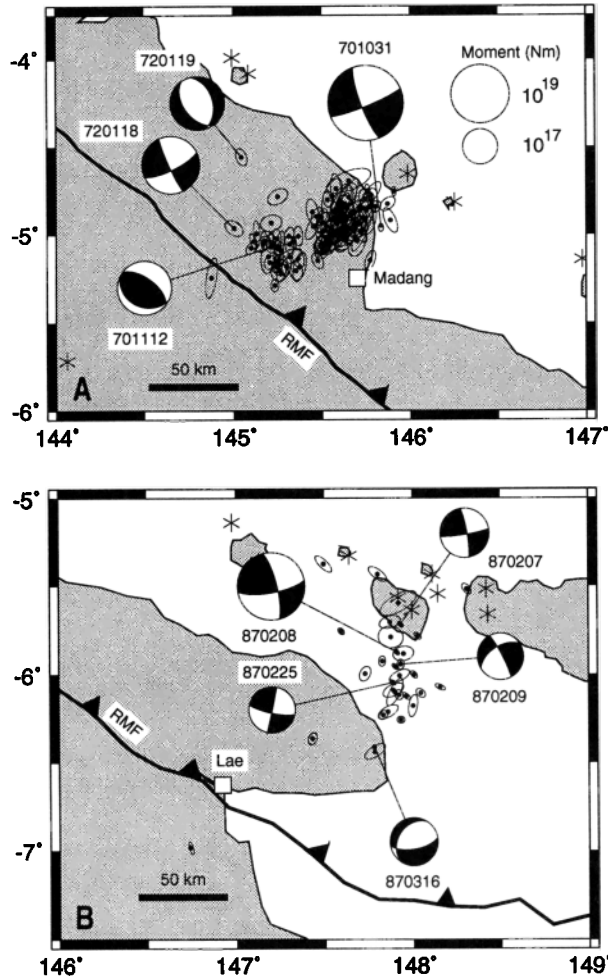


Figure 3. Fault-plane solutions for events in strike slip sequences. (a) 1970 Madang sequence. (b) 1987 Vitiiaz Strait sequence. Aftershocks within (A) 60 days and (B) 15 days are shown with 95% formal confidence ellipses, relocated in model 6 of *Abers and Roecker* [1991]. Symbols same as in Figure 2. Madang aftershock sequence aligns with the left-lateral fault plane of the mainshock, 701031, while Vitiiaz Strait sequence aligns with the right-lateral fault plane of the 870208 mainshock.

Uncertainties

The formal uncertainties determined by least squares inversion (Table 2) are known to drastically underestimate the true uncertainties [e.g., *Nábělek*, 1984]. Several studies have examined different sources of uncertainties of body wave inversion methods [e.g., *Abers and McCaffrey*, 1988; *McCaffrey*, 1988; *Stein and Wiens*, 1986; *Huang et al.*, 1986] and have shown the range of uncertainties expected for simple events. Several tests show that for earthquakes with source durations less than 10 s and recorded by stations in at least two quadrants of the focal sphere (i.e., in both Asia and Australia), strike and rake of mechanisms are generally within 20° for dip-slip mechanisms and 10° for strike-slip mechanisms, dip to within 10°, depth to within 5 km for dip-slip mechanisms and 10 km for strike-slip mechanisms. Seismic moment typically has 20-50% uncertainties. Figure 4 shows that the depth of a moder-

ate-sized thrust earthquake can be determined to within 5 km.

Nodal plane orientations were generally well constrained with uncertainties as quoted above. Near-horizontal thrust planes often have high uncertainties in their strike and rake (Table 2) because large changes in these parameters cause small changes in radiation patterns; the conjugate planes and slip vector orientations are well constrained, as strike and rake trade off nearly completely. Depths for some of the largest events were sometimes poorly determined (± 10 km) because the source pulses were long. In the worst cases, the large strike-slip events (701031, 870208) could be matched at any depths shallower than 15-20 km depth, although the large dip-slip events were better constrained.

The Harvard centroid-moment tensor (CMT) catalog [e.g., *Dziewonski et al.*, 1981] provides independent results for all 15 events in this study occurring since 1977. The CMT technique relies on signal at periods longer than 45-60 s, while the body wave analysis fits signals at shorter periods. The two methods generally determine double-couple orientations that are generally within 10°-20° of one another: 75% of the *P* and *T* axes for events in Table 1 are within 20° of the corresponding CMT solution, and 60% are within 15°. The seismic moments determined by the CMT procedure are on average 30-40% larger, although there is ~50% scatter; similar discrepancies were found for larger sets of solutions from the region [*Abers*, 1989]. There is no indication that the moment discrepancy is largest for the largest earthquakes, as might be expected if the CMT moments include long-period signal that is absent in the body wave analysis [*Ekström*, 1989; *Zhang and Lay*, 1989]. Hence the source of the moment discrepancy is unclear. The long-period CMT data are not very sensitive to depths of shallow earthquakes, so depths were not compared.

Earthquake Relocation

All events in Table 1 are relocated in three-dimensional velocity model 6 of *Abers and Roecker* [1991], except for the 1992 events which are recorded by few (≤ 5) local stations (Figures 2 and 3). Arrival times are taken for regional stations from the ISC catalog and local networks [*Abers and Roecker*, 1991]. Only stations in the Papua New Guinea region are used (ray paths shorter than 600 km), because velocities are less well known for longer ray paths. Depths are fixed at the values determined by waveform inversion. Aftershocks of the Madang and Vitiiaz Strait aftershock sequences are also relocated (Figure 3). Depths are estimated for the Madang aftershocks because several nearby stations were installed and recorded upgoing rays from these events. The Vitiiaz Strait sequence is >100 km from the nearest station, so depths had to be fixed (to 15 km).

The relocations produced two significant changes to the seismicity patterns. First, aftershock epicenters formed well-delineated zones, and the Vitiiaz Strait sequence became 20-40% shorter than the catalog-based aftershock area of *Dmowska et al.* [1991]. Formal confidence ellipses do not show any tendency toward elongation along the inferred fault planes (Figure 3), so the aftershock zone lineations do not obviously reflect errors in relocation. Second, all events near the Huon Peninsula were relocated 15-35 km to the east of their teleseismic locations. Systematic shifts are also seen in ISC catalog residuals, which are ~5 s larger (predicted times earlier)

Table 2. Results From Waveform Inversion

Event	Depth, km	Moment, $\times 10^{18}$ N m	t_{95}^* , s	Strike, deg	Dip, deg	Rake, deg	Slip Az † , deg
661223	22.6 \pm 1.1	4.76 \pm 4.38	5.7	266 \pm 4	56 \pm 2	93 \pm 6	170 \pm 14
670918	33.8 \pm 0.7	0.65 \pm 0.29	3.0	267 \pm 6	43 \pm 1	75 \pm 3	198 \pm 5
701031	8.6 \pm 1.1	274.0 \pm 68.0	40.1	68 \pm 2	83 \pm 2	349 \pm 4	249 \pm 2
701112	22.3 \pm 0.6	3.76 \pm 2.40	5.9	306 \pm 4	59 \pm 1	95 \pm 4	206 \pm 9
720118	26.6 \pm 0.7	7.71 \pm 1.82	13.1	64 \pm 2	76 \pm 2	353 \pm 2	246 \pm 2
720119	9.6 \pm 0.9	4.43 \pm 3.26	4.4	345 \pm 6	42 \pm 1	285 \pm 4	
800625	24.9 \pm 0.7	0.14 \pm 0.18	1.6	280 \pm 26	21 \pm 4	71 \pm 22	209 \pm 4
820914	28.0 \pm 1.8	1.65 \pm 0.30	9.0	289 \pm 51	6 \pm 6	121 \pm 51	168 \pm 7
830311	33.8 \pm 1.0	0.19 \pm 0.07	1.6	40 \pm 7	60 \pm 5	41 \pm 6	
860212a	29.4 \pm 0.6	0.30 \pm 0.22	3.6	248 \pm 8	36 \pm 3	52 \pm 6	202 \pm 4
860212b	28.8 \pm 1.0	0.19 \pm 0.09	4.7	216 \pm 44	16 \pm 6	65 \pm 39	152 \pm 5
870207	8.7 \pm 1.0	1.61 \pm 0.82	3.7	350 \pm 1	82 \pm 2	175 \pm 2	171 \pm 1
870208	11.0 \pm 1.6	54.0 \pm 8.8	20.2	346 \pm 2	77 \pm 4	164 \pm 4	170 \pm 3
870209	20.5 \pm 0.4	0.90 \pm 0.11	3.1	332 \pm 3	84 \pm 3	216 \pm 3	328 \pm 2
870225	23.0 \pm 1.5	0.91 \pm 0.26	2.5	12 \pm 3	89 \pm 2	168 \pm 2	183 \pm 3
870316	7.3 \pm 0.7	1.28 \pm 0.14	13.7	80 \pm 3	65 \pm 3	294 \pm 4	
920221	32.0 \pm 0.5	0.80 \pm 0.01	7.7	254 \pm 9	35 \pm 2	69 \pm 5	189 \pm 5
920227	25.3 \pm 0.5	10.1 \pm 1.0	26.4	248 \pm 8	33 \pm 2	64 \pm 5	188 \pm 4
920515	36.7 \pm 0.7	54.9 \pm 4.0	27.0	242 \pm 5	41 \pm 1	55 \pm 2	195 \pm 3
920521	29.1 \pm 0.9	0.92 \pm 0.14	6.7	303 \pm 7	39 \pm 1	89 \pm 4	214 \pm 4
921218	21.8 \pm 0.6	0.99 \pm 0.33	4.6	254 \pm 20	21 \pm 4	57 \pm 17	198 \pm 4

Uncertainties given are twice the formal error from inversion.

*Duration calculated from second moment of source time function, as 95% of the source pulse.

† Azimuth of slip vector from strike of auxiliary plane, where fault plane has been inferred.

for Papua New Guinea stations to the west than for those to the east. It is unlikely that such a large, systematic residual pattern is attributable to velocity variations along paths to local stations, because perturbations of 10-20% would be needed for P_n ; such large anomalies are not supported by velocity inver-

sion results [Abers and Roecker, 1991]. Rather, the shifts probably reflect a systematic bias in teleseismic locations, perhaps caused by the difference between fast paths to Australian stations [Simpson *et al.*, 1974] and relatively slow paths beneath the Bismarck and Solomon seas.

Waveform Inversion Results

Representative results from waveform inversion (Table 2 and Figures 4 and 5) are discussed here. In the appendix, waveforms are shown and discussed for the six earthquakes occurring before 1977 when digital data were not available.

Dip-slip events beneath the Huon Peninsula. Earthquakes with reverse-faulting solutions are found on both the north and south sides of the Huon Peninsula (Figure 2).

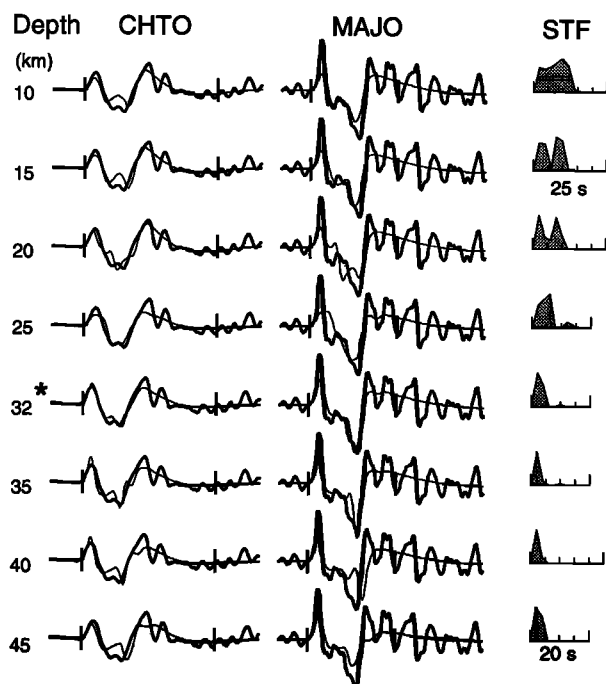


Figure 4. Depth sensitivity of teleseismic waveforms, for typical thrust event (920221) beneath the Huon Peninsula. Waveforms plotted for two stations, showing observed P seismograms (thick lines) and calculated seismograms (thin lines) over a range of depths. Also shown, right, is timescale and source time function (labelled STF) for each depth. Displacement seismograms are rescaled to correct for geometrical spreading and seismic moment. Vertical ticks on seismograms show time window used for inversion. Note separation of direct and surface-reflected phases (pP , sP) increase with depth. Although the source duration shows significant trade-off with depth, waveforms are not fit well at depths more than 3-5 km different from depth determined by inversion (asterisk).

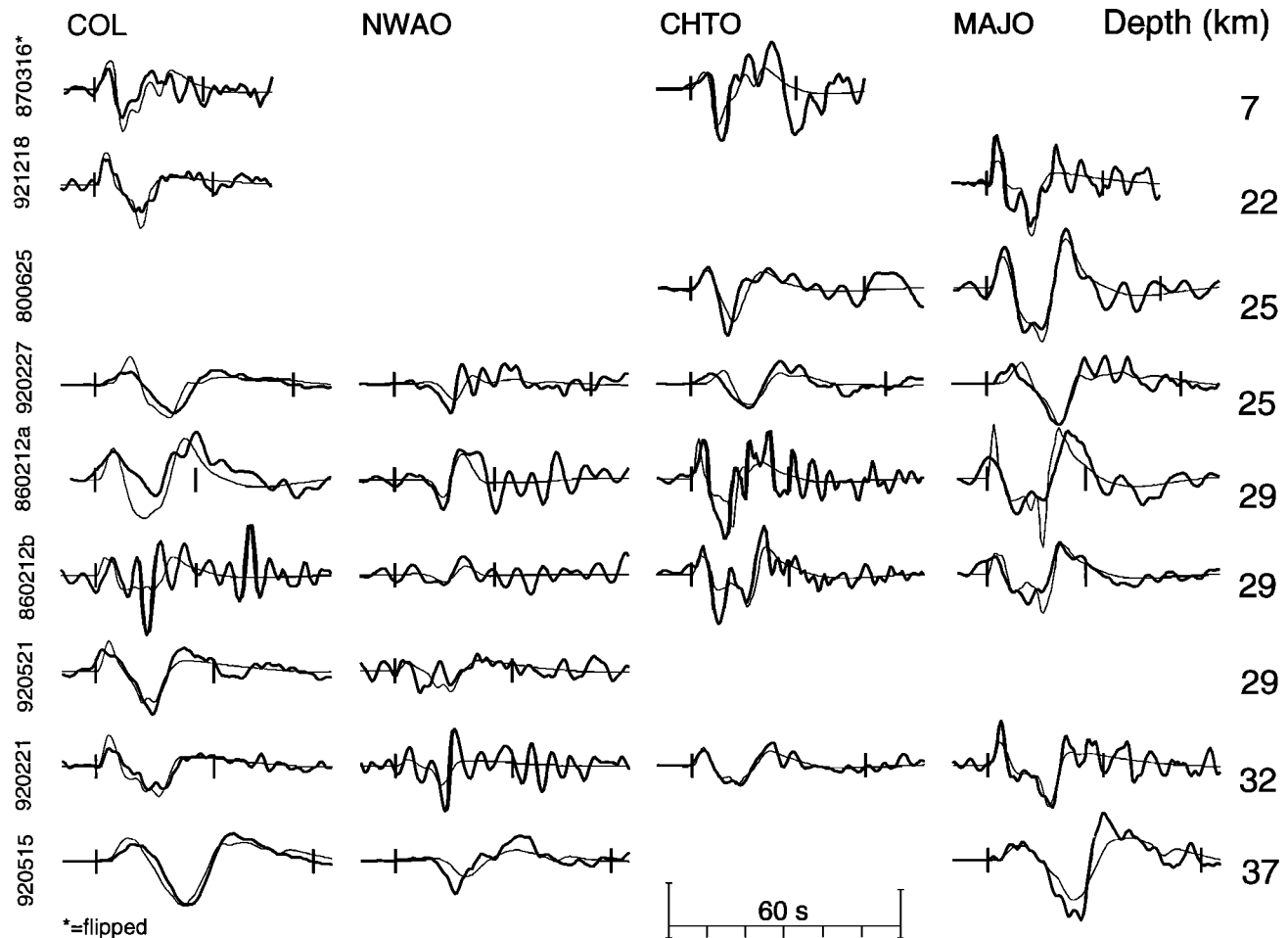


Figure 5. Representative *P*-wave seismograms for dip-slip earthquakes in Huon region. Four digital stations are shown (top), ordered by source depth (right). Events are labeled (left) as in Table 2. Other symbols and scaling same as Figure 4. Note seismograms for normal-faulting event 870316 are flipped to have same polarity as thrust events. Depth phases produce distinct late pulses for smaller earthquakes (e.g., 920221 and 921218) but cannot be easily distinguished for the largest earthquakes with long source durations (920515 and 920227).

The two largest thrust events 920227 and 920515 have $M_0 > 10^{19}$ N m. They had half-durations near 12 s (Table 2) and probably ruptured faults that are ~ 75 km in length (for simple bilateral faulting and rupture velocities of ~ 3 km s^{-1}). Although the uncertainty in interpreting source dimension from source-time function may be as much as 50%, the expected fault areas are comparable in size to the area of the Huon Peninsula. Thus these two events represent movement on a significant regional fault.

Events on the north side of the Huon Peninsula are 25-37 km deep, compared with 22-27 km depths for events on the south side of Peninsula, a resolvable difference given uncertainties less than 5 km (Figure 4). Figure 5 shows *P* waves recorded at four stations, for all dip-slip events, ordered by increasing depth (seismograms for normal-faulting event 870316 are flipped so that it appears to have the same polarity as the thrust events). The depth is constrained by the time difference between direct (*P*) and reflected (*pP*, *sP*) arrivals on the *P* wave train, which appear as distinct pulses for most of these events (the initial upward pulse is the direct *P*, while the sec-

ond pulse dominated by an upswing is the combined *pP* and *sP*). These pulses are not separated for event 870316 at 7 km depth, or for the largest two events which have the longest source durations. Almost all of the events in Figure 5 have smaller signals at station NWAO (in southwest Australia) than elsewhere. NWAO is closer to a nodal plane than the other stations, and as a consequence the north dipping plane has a shallow dip for nearly all of these events.

Vitiaz Straits Sequence (870207-870225). Event 870208 ($M_S = 7.4$) was one of the largest recent earthquakes in eastern New Guinea [King *et al.*, 1987; Dmowska *et al.*, 1991]. It was preceded by one major foreshock (event 870207) and two large aftershocks (870209 and 870225) (Figure 3b). In addition, the only known normal faulting earthquakes in the Huon Peninsula occurred 36 days after the mainshock (870316 and nearby events in the CMT catalog, not shown). Solutions for the all other events are strike slip. Aftershocks show a N-S alignment and implicate the right-lateral nodal plane as the fault plane [Dmowska *et al.*, 1991]. The fault plane solution for the main shock is similar to the CMT mechanism ($\sim 10^\circ$ dif-

ference in principal axes), although the moment is half the CMT moment. Depths for all these events are in the upper 25 km, and waveforms clearly rule out the ISC depth of 62 km for the main shock or 40 and 47 km for the two aftershocks. (Arrival times do not constrain depths very well here, probably because ray paths to regional stations are nearly horizontal for shallow earthquakes except near Lae [Abers and Roecker, 1991].)

Lae Area Gravity Survey

Data. In conjunction with a micro-earthquake survey [Kulig *et al.*, 1994], gravity measurements were made in the Lae area (Figure 6). Measurements were taken with a Lacoste-Romberg gravity meter, with methods that were repeatable to 0.3-0.7 mGal on successive days. One traverse extends from the Markham River 30 km to the north, with cross-lines through the city of Lae and along the Markham Valley (RMF in Figures 1 and 3). Stations in Lae and in the Markham Valley were measured at permanent survey markers or along the shoreline. Station locations and elevations north of Lae were surveyed at 1-km intervals by the Papua New Guinea University of Technology Surveying Department. Surveying was necessary to minimize errors in station elevation in mountainous terrain and provides sufficient vertical control (within 1-3 m) to keep gravity anomaly uncertainties to less than 1 mGal. All gravity measurements were corrected to a value of 977,996.7 mGal at station "LAE-M" of the Australian gravity grid, at the Lae airstrip [Wellman *et al.*, 1974] and thus are tied to the IGSN-71 reference system. The actual LAE-M marker was paved over, but sufficient reference marks existed to determine its location to 1 m.

Measurements (Table 3) are corrected for instrument drift, adjusted to the tie value and corrected for latitude, elevation, and terrain using standard methods [Telford *et al.*, 1976]. Data

are reduced to the GRS 67 formula [e.g., Woollard, 1979], and Bouguer anomalies are reduced to a density of 2670 kg m⁻³. Terrain corrections are determined using the Hammer-chart method [Telford *et al.*, 1976], with elevations estimated in the field to 50 m, manually from 1:100,000 scale topographic maps to 9.9 km, and from a hand-digitized 2.5-min grid out to 37 km. Terrain corrections vary from 1.6 to 10.3 mGal and generally increase with elevation. Uncertainties in these corrections are estimated to be 10-20%, mostly because of occasional extreme and unexpected relief at scales of 50-200 m. Thus the complete Bouguer anomalies (CBAs) have uncertainties of 1-3 mGal.

Results. The major feature observed, discussed below, is a steep negative gradient to the northeast from Lae. Gravity values also increase along strike to the southeast (Table 3), consistent with high values (+100 to +150 mGal) reported over the Papuan Ultramafic Belt along the northeast coast of the Papuan Peninsula [Milsom, 1973]. Additional control in the Papuan Peninsula is provided by *St. John* [1967, 1970], south of the Markham Valley near 146.6°E (Figure 6). However, the presence of the along-strike gradient makes the southern measurements difficult to use with the Lae survey data, and their gravity values (-60 to -100 mGal) are probably lower than would be found in a continuous transect through Lae. High Bouguer anomaly values for the Huon Peninsula (+50 mGal) are shown on gravity maps for the region [e.g., Bureau of Mineral Resources, 1979], but only one point measurement could be found that is consistent with this high, from *St. John's* [1967] original survey. Likewise, *St. John* [1967] reports only three additional CBA values from the Finisterre-Huon interior, with terrain corrections as large as 80 mGal. Hence little reliable constraint exists on the gravity field northeast or east of the Lae survey.

Discussion

Thrust System Beneath the Huon Peninsula

Active Tectonics. The Huon-Finisterre earthquakes are a consequence of continued overthrusting of the Finisterre volcanic arc terrane on the northern margin of Australia. Thrust mechanisms (Figures 2 and 7a) show both high-angle and low-angle faulting with slip vectors perpendicular to the RM fault or its eastern extension, the New Britain trench (Figure 7b). They provide direct evidence for compression on the RM fault system [e.g., Davies *et al.*, 1987; Rogerson *et al.*, 1988] and are inconsistent with the hypothesis that the Ramu-Markham fault is strike slip (as suggested by Dow [1977], Hamilton [1979], Cullen and Pigott [1989] and others).

The two largest thrust earthquakes, 920227 and 920515, have seismic moments of 10¹⁹ N m and 5 × 10¹⁹ N m, 25-35 km deep beneath the northern Huon Peninsula. These moments are comparable to the largest strike-slip events in the region and are 1-3 orders of magnitude larger than other thrust events in eastern New Guinea (Table 2) [Abers and McCaffrey, 1988]. Although there is no direct evidence supporting one fault plane over the other, nearly all reported surface thrust faults dip to the north or northeast in the region [e.g., Davies *et al.*, 1987; Rogerson *et al.*, 1988; Abbott and Silver, 1991] and no evidence for a south dipping zone has been found north of the FH

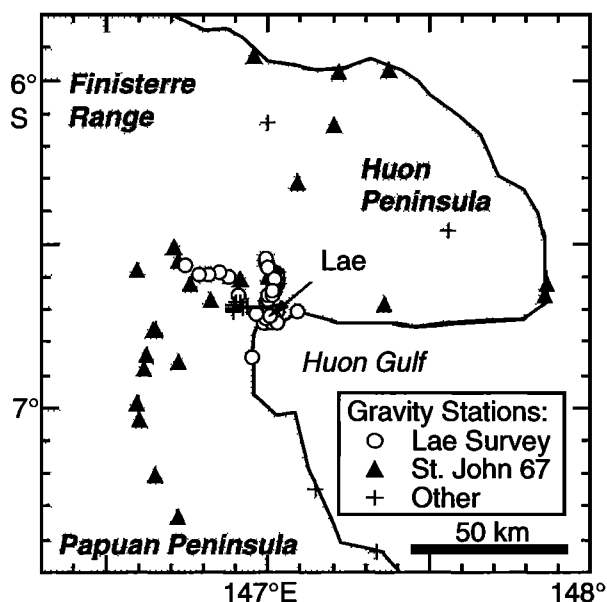


Figure 6. Locations of gravity stations. Lae survey observations given in Table 3, others from *St. John* [1967] or other sources [e.g., Pettifer, 1974].

Table 3. New Gravity Measurements From Lae Area

Station	Latitude, °S	Longitude, °E	Elevation, m	Gravity, mGal	Free-Air Anomaly, mGal	Simple Bouguer, mGal	Corrected Bouguer, mGal
01	6.6763	146.9911	53.0	977969.71	-115.5	-121.5	-119.5
03	6.7356	146.9989	10.2	977996.71	-103.0	-104.1	-102.3
04	6.7182	146.9950	21.2	977986.68	-109.3	-111.6	-110.0
06	6.6435	147.0151	121.2	977958.54	-105.0	-118.6	-115.2
07	6.6372	147.0214	147.5	977954.08	-101.2	-117.7	-114.3
08	6.6284	147.0211	178.3	977945.56	-100.0	-120.0	-116.2
09	6.6198	147.0233	169.6	977944.49	-103.6	-122.6	-117.4
10	6.6133	147.0245	140.6	977948.46	-108.5	-124.2	-116.6
11	6.6728	146.9968	57.5	977969.74	-114.1	-120.5	-118.5
12	6.6074	147.0238	189.1	977936.82	-105.0	-126.2	-119.0
13	6.6037	147.0219	269.9	977920.08	-96.8	-127.0	-121.3
14	6.6596	146.9955	67.6	977964.97	-115.4	-123.0	-120.7
15	6.7431	146.9914	1.5	977998.09	-104.5	-104.6	-102.7
16	6.7395	146.9801	0.7	977994.72	-108.0	-108.1	-106.5
17	6.7401	147.0083	0.3	978001.31	-101.6	-101.6	-99.0
18	6.5966	147.0223	309.9	977909.67	-94.7	-129.4	-123.0
19	6.5881	147.0169	302.6	977908.93	-97.5	-131.4	-125.8
20	6.5831	147.0095	276.7	977910.07	-104.2	-135.2	-129.0
21	6.5777	147.0033	239.1	977913.82	-112.0	-138.8	-131.7
22	6.5677	146.9965	232.5	977911.08	-116.6	-142.6	-134.3
23	6.5603	146.9911	312.1	977896.20	-106.7	-141.7	-133.1
24	6.5517	146.9886	377.6	977878.41	-104.1	-146.4	-136.3
25	6.5447	146.9903	467.1	977860.75	-94.0	-146.4	-136.5
26	6.5411	146.9912	557.8	977841.66	-85.1	-147.6	-137.3
27	6.5729	146.9987	240.6	977911.84	-113.4	-140.3	-132.6
28	6.6100	147.0212	242.5	977927.29	-98.1	-125.3	-119.9
29	6.7108	146.9948	26.5	977984.05	-110.1	-113.1	-111.4
30	6.7243	146.9882	18.5	977989.32	-107.6	-109.7	-108.1
31	6.7076	147.0255	26.6	977992.50	-101.5	-104.5	-102.6
32	6.7275	147.0152	10.8	977995.99	-103.4	-104.6	-102.7
33	6.6604	147.0127	71.5	977970.77	-108.4	-116.5	-114.0
34	6.6436	147.0087	90.1	977962.68	-110.5	-120.5	-117.4
35	6.7395	147.0256	1.5	978004.44	-98.0	-98.2	-94.2
36	6.7126	146.9641	11.9	977980.84	-117.8	-119.2	-117.3
37	6.6777	146.9139	22.7	977971.14	-123.5	-126.0	-123.7
38	6.6600	146.9039	34.1	977967.07	-123.7	-127.5	-125.1
39	6.7179	147.0073	17.0	977989.45	-107.8	-109.7	-108.0
40	6.8503	146.9448	1.5	978027.75	-77.1	-77.2	-74.2
41	6.7070	147.0887	0.5	978011.78	-90.3	-90.4	-86.2
42	6.6013	146.8748	46.1	977955.39	-130.4	-135.6	-132.4
43	6.5870	146.8453	36.1	977960.13	-128.5	-132.5	-129.7
44	6.5967	146.8093	27.7	977975.87	-115.5	-118.6	-116.5
45	6.5964	146.7828	36.1	977968.41	-120.4	-124.4	-122.6
46	6.5643	146.7425	69.5	977942.14	-135.7	-143.5	-141.4

terrane. Thus it is more likely that these earthquakes represent slip on northeast dipping faults (e.g., Figure 7a).

The north Huon events (>50 km from the RM fault) and the south Huon events (<50 km from the fault) do not lie on a single fault plane that reaches the surface at the RM fault zone. The two groups of events are at similar depths, but the south Huon events are almost directly below the RM fault system; they are too deep and the dips of their north dipping nodal planes are too small to be directly related to faults in the Markham Valley. Thus although the north Huon events can represent slip on a down dip extension of the Ramu-Markham

fault, the south Huon earthquakes do not. One possibility (Figure 8) is that the south Huon events show slip on a down dip extension of the Highlands thrust belt to the south. Microseismicity [Kulig *et al.*, 1994] shows that vertically dipping faults are active above the south Huon events and terminate to the south at the Markham Valley. Their southern limit is evidence that some major structure reaches the surface near the Markham Valley, but the geometry of such a structure and its relation to the south Huon events is unclear.

Possible mechanism of terrace uplift. The north Huon earthquakes lie directly below a large sequence of uplifted

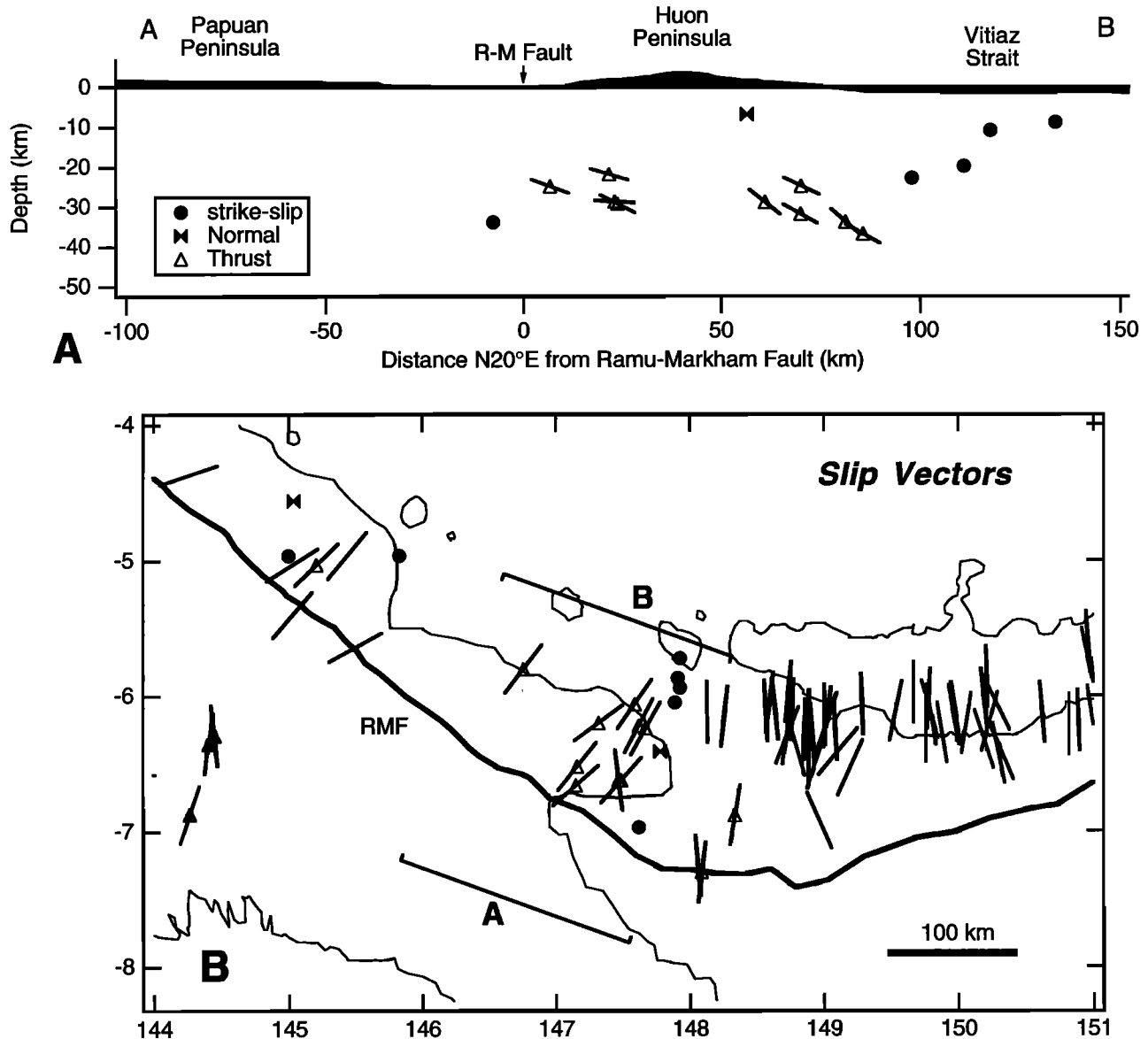


Figure 7. (a) Cross section showing large earthquakes and topography over Huon peninsula. R-M Fault is the surface trace of the Ramu-Markham fault. Horizontal scale, in kilometers, gives distance X north from thrust front. For thrust earthquakes, north dipping nodal plane is projected onto section and plotted as short line segment. North Huon events, $X = 60-90$ km, are consistent with thrust faulting on the R-M fault, while south Huon earthquakes, $X = 5-25$ km, project to the surface farther south. (b) Slip vector azimuths for thrust earthquakes. Triangles show thrust earthquakes from this study and Abers and McCaffrey [1988], lines without symbols show slip vector azimuths taken from CMT catalog for New Britain trench subduction earthquakes or Ramu-Markham thrust earthquakes. The thick solid line (RMF) shows surface trace of Ramu-Markham fault and New Britain trench.

Pleistocene coral terraces along the north and east coasts of the Huon Peninsula [Chappell, 1974]. Slip on the faults that generated the north Huon earthquakes may be responsible for the terrace uplift, since the terraces are almost directly over the earthquakes and the earthquakes show substantial vertical displacement. The terraces have been uplifting at a rate of $1-3 \text{ mm yr}^{-1}$ for the last $\sim 10^5$ yr. By comparison, the summed seismic moment of the 1992 north Huon earthquakes is $\sim 6 \times$

10^{19} N m . If the seismic moment is uniformly distributed over a fault 75 km by 25 km in area, then the total slip is $\sim 1.1 \text{ m}$ (following Brune [1968]). On a fault dipping 35° , the corresponding crustal thickening is 0.6 m , and an earthquake as large as the 1992 events every 200-600 years is sufficient to produce the observed uplift. However, some form of isostatic compensation is expected to occur at these timescales. For Airy compensation and typical crustal densities, the surface

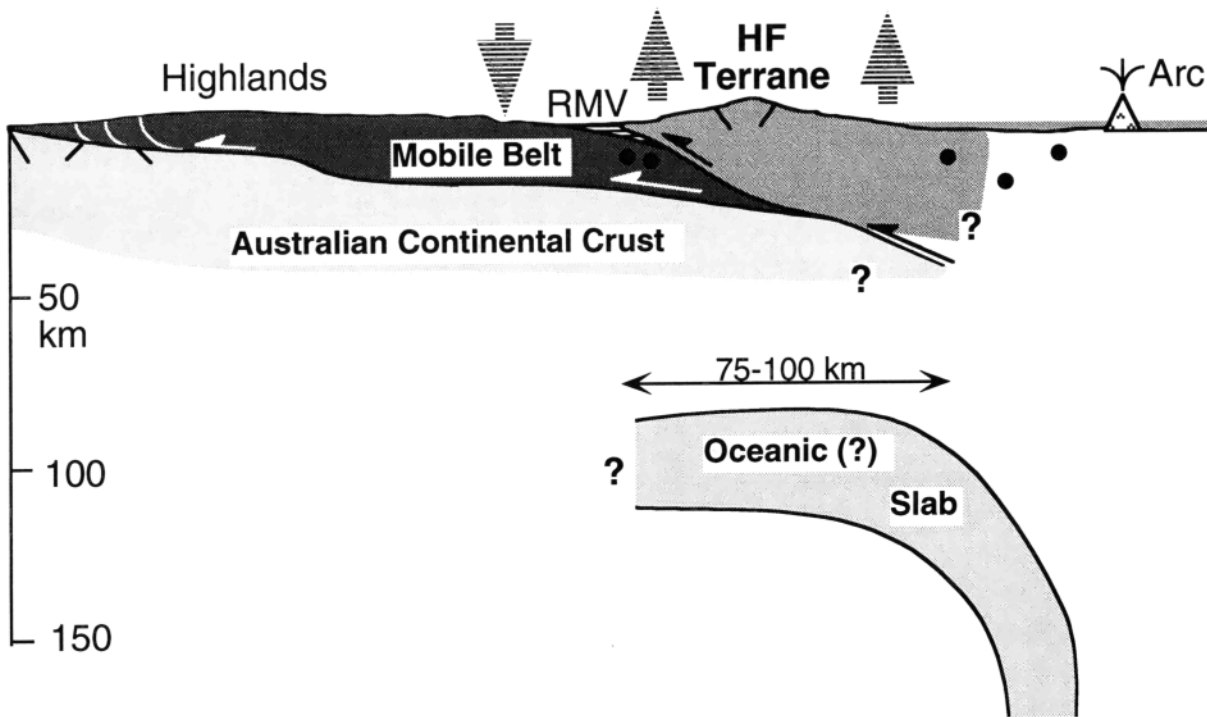


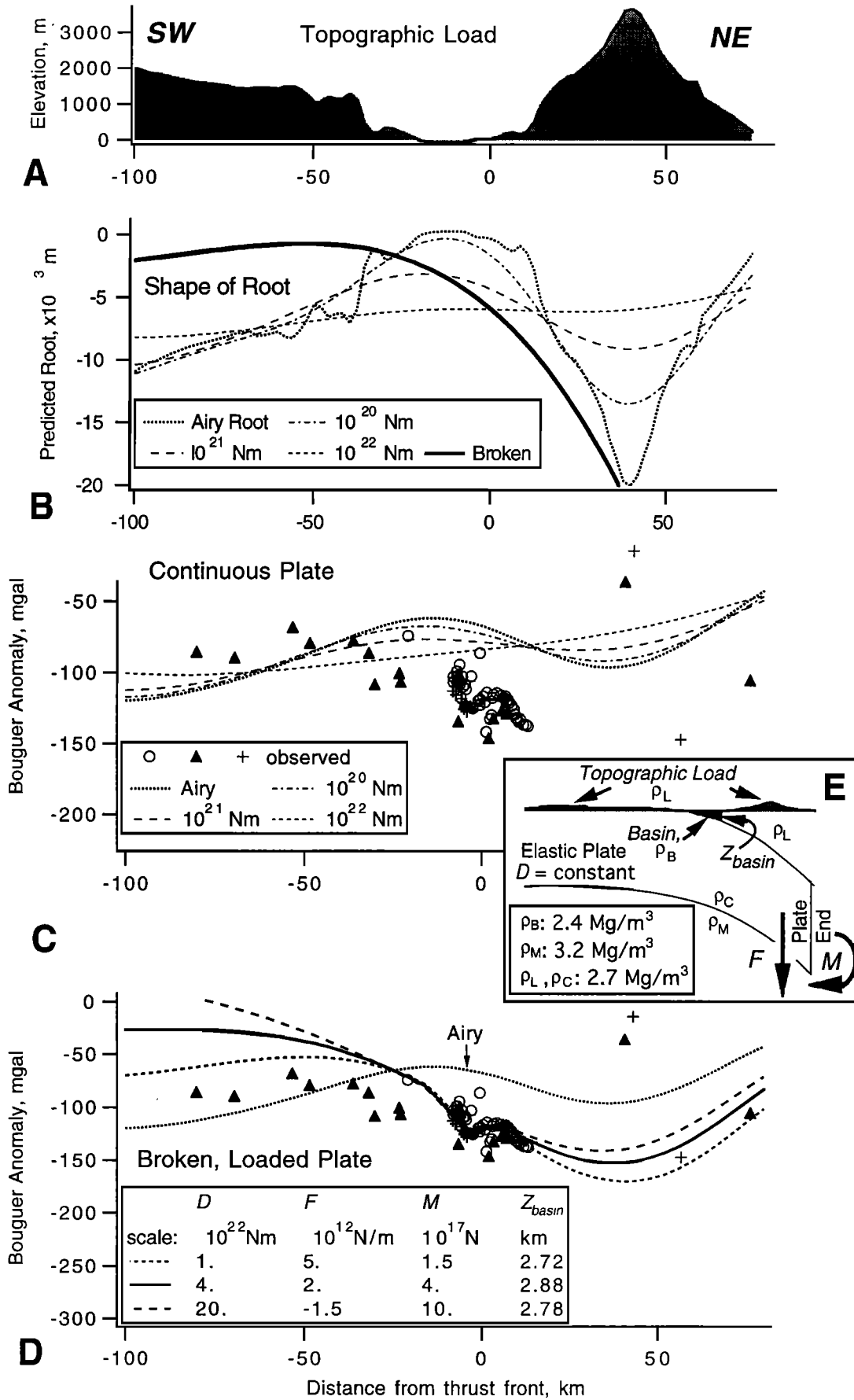
Figure 8. Cartoon cross section showing inferred geometry of Huon-New Guinea collision. RMV denotes Ramu-Markham valley, and solid circles indicate inferred locations of cross faults from Figure 3b (Vitiav Strait sequence) and from *Kulig et al.* [1994] (Lae microearthquake survey). Deep slab geometry is inferred from seismicity [Abers and Roecker, 1991]. Large shaded arrows show observed sense of vertical motions, uplift of terraces on the north Huon Peninsula [Chappell, 1974], of markers along the Ramu-Markham fault [Crook, 1986; Silver et al., 1991], and subsidence of drowned coral reefs near the north coast of the Papuan Peninsula [von der Borch, 1972; Silver et al., 1992]. The north Huon earthquakes are 75-100 km north of the south extent of intermediate-depth seismicity, suggesting that Australia has overridden the slab by at least this much.

uplift is likely to be 6-7 times smaller than the crustal thickening (regional compensation may give different values but would still act to reduce uplift). Thus earthquakes similar to the 1992 north Huon events would have to occur every 30-100 years to raise the terraces. Hence reasonable recurrence times

of similar sized earthquakes could produce the terraces, although the actual recurrence times are clearly speculative.

Compilations of large, pre-1970 earthquakes [Everingham, 1974] show three candidates for previous Huon Peninsula events: October 2, 1906, February 3, 1907, and May 12,

Figure 9. Observed gravity and calculations. Cross section is parallel to A-B on Figure 7. (a) topographic load, from a hand-digitized 2.5-min grid for $X > -75$ km and global digital topography models farther south. (b) Shape of root predicted by elastic plates. Thin lines for continuous plates and a range of flexural rigidity (D) values, shown. Any plate with $D \geq 10^{22}$ N m predicts a south dipping root beneath the Ramu-Markham valley, opposite to what is inferred from gravity. "Broken" is root for loaded, broken-plate solution in Figure 9d, with $D = 4 \times 10^{22}$ N m. (c) Bouguer anomalies, showing gravity observed (symbols) and calculated for continuous elastic plate (lines). "Airy" is result for $D = 0$. Data symbols are the same as Figure 6; all values include terrain corrections. Calculations assume a 30 km depth to moho corresponding to zero deflection, and densities (ρ) appear as shown in Figure 9e. Flexure is calculated by applying appropriate filter to topography in the Fourier transform domain, and gravity is calculated by a polygon method from digitized flexural root [Talwani et al., 1959]. Constant long-wavelength field of 25 mGal is added to all calculated values [Abers and Lyon-Caen, 1990]. (d) Gravity fits for three broken, loaded plate models which match the Lae survey data. Elastic plate deflections calculated for line force (F) and bending moment (M) applied at plate end at $X = 70$ km, illustrated in 9e. Values listed for D , F , M , and Z_{basin} , the maximum predicted basin depth. Flexure is calculated similar to Figure 9c, with added homogeneous solution for M, F boundary conditions at $X = 70$ km and finite deflection as X approaches $-\infty$. Negative load of low-density basin sediments (ρ_B) is iteratively added to topographic load, with a basin shape paralleling calculated deflection as shown; anomaly of basin is included in calculated gravity. Lyon-Caen and Molnar [1983] give further details. (e) Geometry and sign conventions used in broken plate calculations.



1938. These are the only shallow events with magnitude greater than 7.0 within 150 km of 920515. Because of uncertainties in location, depth, and focal mechanism, we cannot say whether or not these events were similar to the 1992 sequence (for example, they may have been similar to the 1987 strike-slip sequence). Still, 2-4 such events per century could maintain the observed terrace uplift rates.

In most subduction zones, thrust earthquakes imply a large component of vertical thickening associated with each earthquake, but because additional forces are active (e.g., slab pull) there is often no long-term uplift. Some differences are needed to explain the presence of the Huon terraces and the absence of similar terraces at most other subduction zones. One possibility is that continental convergence is more likely to produce crustal thickening than oceanic plates, because continental crust is difficult to subduct [e.g., *Molnar and Gray, 1979*]. Buoyant continents would thicken, while dense oceans would more likely sink into the mantle. Terrace uplift may be evidence that shortening is accommodated by crustal thickening of the Australian continental crust more than by subduction.

Depths of terrane-bounding faults. The north Huon events represent significant slip over a large fault zone (tens of kilometers wide). These events may delineate the fault surface upon which the HF terrane is being emplaced and could represent the same thrust system that reaches the surface in the RM Valley [*Silver et al., 1991*]. The events are 25-40 km deep, and most are near 30 km deep. This suggests that the collision involves the entire crust of the old arc but little of its underlying mantle. The depths are much deeper than detachments observed in other arc-continent collisions in the geological record, such as in Alaska or in the southern Appalachians, where terranes seem to be only 10-15 km thick [e.g., *Cook et al., 1979; Plafker et al., 1989*]. However, the mountains produced by those thrust systems have been largely removed by erosion. The depth of the inactive faults has been much reduced by eroding the overlying mountains, and by the consequent isostatic rebound. If the HF ranges were eroded to sea level, then the faults now producing the earthquakes would be elevated by isostasy a substantial distance toward the surface, and simple calculations suggest that 10-15 km of exhumation is not unreasonable. Hence it is possible that the HF earthquakes represent common depths of active terrane-bounding thrust faults.

Gravity, Isostasy, and Plate Flexure

Above a compensation depth, the New Guinea collision zone is expected to isostatically balance the adjacent Australian craton which has elevations near sea level [*Abers and Lyon-Caen, 1990*], so (neglecting major mantle density changes) the New Guinea topography above sea level is an excess load that is somehow compensated. However, calculations show that local isostatic compensation does not produce the steep gravity gradient and large negative Bouguer anomalies observed near Lae (Figure 9). Regional compensation mechanisms which support regional topography by an unbroken elastic plate also matches the observed gravity poorly, and for reasonable flexural rigidities ($D \geq 10^{22}$ N m) a gradient of opposite sign is predicted (Figure 9c). The Papuan Peninsula/New Guinea Highlands topography contains more volume than the HF range topography, so continuous elastic plates produce a south dipping moho beneath the Markham

Valley. A southward gradient is not observed, so forces other than the weight of topography are necessary to produce the observed gravity signal.

Collisional geometry is better explained as a broken elastic plate underlying the topography [e.g., *Lyon-Caen and Molnar, 1983*]. Added loads are accounted for by applying an additional line force (F) and bending moment (M) to the end of the plate (Figures 9d and 9e), and by including a low-density RM basin overlying the flexed plate (Figure 9e). For broken plates, a variety of flexural rigidities (D), applied moments (M), and line forces (F) are consistent with gravity observations (Figure 9d). Either M or F must be positive to produce the observed gravity gradient (Figure 9e shows sign conventions), and imply an additional downward load of some form. Plates with $D < 10^{21}$ N m have flexural wavelengths that are too small to produce the observed gravity low, and plates with $D > 5 \times 10^{23}$ N m do not produce a northward dip beneath the Markham Valley.

In all cases where the gravity "step" between -5 and 5 km is matched, the predicted deflection change across the basin (Z_{basin}) is 2-4 km. Thus consistent loads or moments can produce a basin 2-4 km deep. The along-strike gradient is not accounted for in modeling points south and north of the basin together, and when a gradient is included, Z_{basin} may reach 6 km and still match gravity (not shown). A basin depth of 5 km is consistent with the shape of teleseismic waveforms for nearby earthquakes, discussed above.

The values of M and F suggest several candidate mechanisms for generating the excess load, such as pull from a subducted slab or from obducted mantle slivers. A slab 200 km long and 50 km wide is consistent with seismicity (Figure 8), and if 50 kg m^{-3} denser than the surrounding mantle would correspond to a force per unit length of 5×10^{12} N m^{-1} . A 100-km moment arm to its center of mass would produce a moment per unit length of 5×10^{17} N. Alternatively, the HF fault zone may thrust dense mantle rocks over crustal rocks and generate a load. A triangular mantle wedge 50 km long and 25 km thick, that is 500 kg m^{-3} denser than the crust, would have a sufficient weight (per along-strike length) of 3×10^{12} N m^{-1} . Whatever the cause, additional loads comparable to the topographic loads are needed to produce the observed gravity values and gradients.

Strike-Slip and Normal Faulting

Two significant strike-slip event sequences are observed (Figure 3). Both are less than 25 km deep, shallower than most thrust earthquakes, are confined to the northeast side of the RM fault zone, and are southwest of active volcanoes offshore. Related deformation is also indicated by the 1985 Biella earthquake and aftershocks, which show left-slip faulting on an E-W striking fault in central New Britain [*Mori et al., 1987*]. Relocated aftershocks for the two events (Figure 3) are elongated along one of the fault planes, along the left-lateral plane for the 1970 sequence and along the right-lateral plane for the 1987 sequence. The probable fault planes then intersect the RM fault at a high angle, unlike strike-slip events in the New Guinea Highlands [*Abers and McCaffrey, 1988*] or strike-slip faults in other island arcs [e.g., *Fitch, 1972*] which are parallel to major thrust systems.

The large strike-slip events have slip vectors that represent

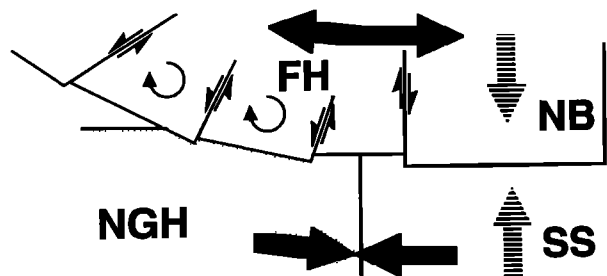


Figure 10. Possible relationship between strike-slip faulting on the north side of the Ramu-Markham fault and the eastern limit of continent collision. Strike-slip faults may accommodate small amounts of adjustment and rotation of upper plate, in the region of continental collision where resistance to subduction is high. Slip vector changes require some combination of along-strike extension of the upper plate and along-strike convergence of the lower plate, at combined rates roughly half of subduction velocity at New Britain trench.

displacement in the same direction as the associated thrust fault system (Figures 2, 3 and 7b). Hence the strike-slip events do not represent slip partitioning. Possibly, they represent transfer structures or tear faults (fault zones that transfer slip between different thrust surfaces). However, the Vitiaz Strait earthquakes are above the Huon thrust system (Figure 7a), so are internal to the HF block rather than on its boundary. More likely, these events represent small tears within the overriding plate allowing New Britain to move south relative to the Huon Peninsula and allowing the HF block to deform (Figure 10).

Both strike-slip sequences include normal-faulting aftershocks. The normal-faulting earthquakes have shallow depths (<10 km) and are located near the crests of the accreting ranges (e.g., Figures 3 and 7). Several normal faults and tilted fault blocks have been mapped in the northern Huon Peninsula [Robinson, 1974], and potential normal faults have been identified farther west (L.D. Abbott, Structure of the Finisterre arc-continent collision zone of northern Papua New Guinea, sub-

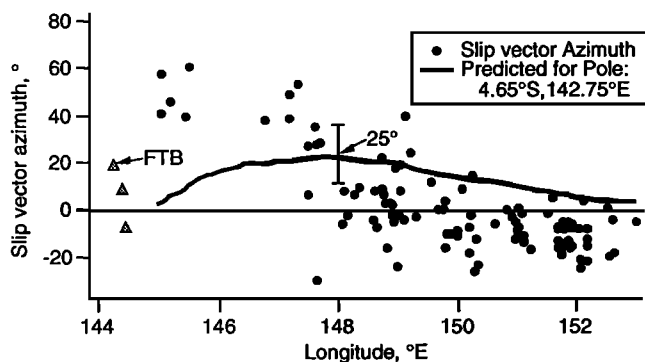


Figure 11. Slip vector azimuth versus longitude for thrust earthquakes, from Figure 7b. Solid line shows slip azimuth predicted for a single pole, calculated along a line 50 km north of the thrust front. HF region vectors, west of 148°E, show a $\geq 25^\circ$ more easterly azimuth than New Britain vectors. The discrepancy cannot be explained as rotation about a single pole. Triangles show slip vectors within the Highlands [Abers and McCaffrey, 1988] and were not used in fit.

mitted to *Tectonics*, hereinafter referred to as Abbott, submitted manuscript, 1993). Possibly, the normal faulting is caused by flexing of the arc terrane as it folds over the crustal-scale thrust ramp. Alternatively, the topography at the range crest may generate excess vertical load that locally exceeds horizontal stresses, in the manner suggested by *Dalmayrac and Molnar* [1981]. The geometry of deformation here is complex, and additional information is needed to determine the extent of these faults and their relationship to topography.

Earthquakes near Madang (Figure 3a) and near Lae [Kulig *et al.*, 1994] suggest that the HF block is broken up by many strike-slip faults. One additional range-perpendicular fault with left-lateral motion has been found from field mapping (Abbott, submitted manuscript, 1993) and others seem likely. Numerous strike-slip faults would produce rotations within the Huon Peninsula as it docks (Figure 10). Left-lateral faulting is consistent with clockwise paleomagnetic rotation, which is observed for the Huon Peninsula in the last 4-5 Ma [Falvey and Prichard, 1982]. The overall pattern suggests that convergence in the Lae region is impeded (Figure 10). Such deformation is expected if the continental collision with Australia is more resistant to compression than is oceanic subduction at the New

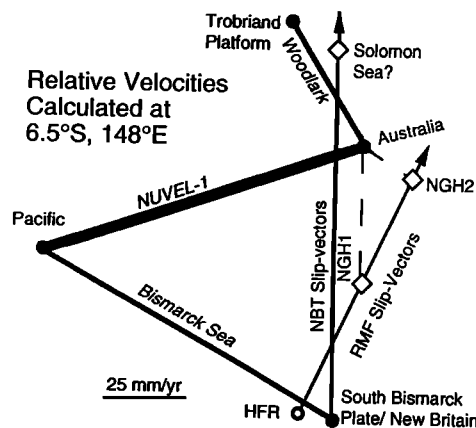


Figure 12. Relative velocities of plates and blocks in the Huon region. Figure 1 shows locations of blocks and bounding structures. Solid circles and thick lines show velocities constrained by magnetic lineations, as labeled. Scale shown in lower left. Diamonds denote velocities constrained only by slip vector azimuths. Key: HFR, Huon-Finisterre Ranges; NBT, New Britain Trench; RMF, Ramu-Markham fault; and NGH, New Guinea Highlands. Velocities calculated from Euler poles for Pacific-Australia motion [DeMets *et al.*, 1990], Pacific-South Bismarck motion [Taylor, 1979], and Woodlark basin extension. Woodlark Euler pole is estimated to be $14^\circ\text{S}, 136^\circ\text{E}$, at $1.75^\circ/\text{Ma}$, from velocities of *Weissel et al.* [1982, Figure 8] and the 10% reduction in spreading rate from 155°E to 153°E . Slip vector azimuths, from Figure 11, give Solomon Sea and NGH velocity azimuths relative to South Bismarck/New Britain plate. The slip discrepancy (Figure 11) is partitioned into $\sim 10 \text{ mm yr}^{-1}$ Huon region along-strike extension and the rest as deformation south of the RM Fault; smaller extension rates would give higher NGH-Australia discrepancies. Motion between the Caroline plate [Weissel and Anderson, 1978] was ignored because it is probably small and because it degrades further the internal matches.

Britain Trench, because continental crust is buoyant and resists subduction. Deformation in the continental collision will be distributed rather than localized as at the New Britain trench, and will result in some migration of the trench relative to the RM fault zone.

Slip vector discrepancies and plate motions

A discrepancy of 20°-30° exists between slip vector azimuths for subduction earthquakes east of 148°E, and the earthquakes west of 148°E (Figure 11). The discrepancy cannot be explained by a nearby pole of plate rotation, and a pole determined by a least squares fit to the slip azimuths shows systematic mismatch to vectors west of 148°E. The discrepancy requires additional deformation, either in the southern footwall or in the northern hanging wall (Figure 10), with overall velocities near 50 mm yr⁻¹ for reasonable subduction rates at New Britain (Figure 12).

Deformation south of the RM fault would imply that the New Guinea Highlands move east relative to the Solomon Sea, for example, by strike-slip motion near the Trobriand trough [e.g., *Kirchoff-Stein*, 1992] or by E-W shortening along the Aure trough [e.g., *Kugler*, 1993]. However, rates of only a few millimeters per year have been found along either structure, and are not obviously sufficient. An additional zone of E-W convergence or plate boundary is needed, if the slip vector discrepancy is explained by deformation south of the RM fault.

Calculations of simple strain fields can be used to compare boundary velocities to observed paleomagnetic rotations within the HF block. *McKenzie and Jackson* [1983] derive a simple relationship for uniformly deforming regions, between rotation rates measured on small blocks and the velocities of the region's boundaries, which we use here. If the entire slip vector discrepancy is taken up in the HF block, then 50 mm yr⁻¹ of right-lateral shear is distributed uniformly over a 50-km-wide deforming HF terrane. These values give clockwise rotation rates of ~30°/Ma. This rate is an order of magnitude higher than the 15° clockwise rotation observed in 4-5 Ma [*Falvey and Prichard*, 1982] and suggests that the slip vector discrepancy is much too large to be accommodated by shear of the overlying plate. Still, causative faults have not been identified for an alternative scenario.

The need for additional deformation is also inferred by attempting to construct a consistent set of regional velocities (Figure 12, see caption for constraints), most likely south of the RM Fault. The velocity field does not reproduce well the observed N-S convergence between Australia and the New Guinea Highlands, suggested by earthquake slip vectors (Figures 7b and 12). The Highlands slip vectors require high velocities and ~50 mm yr⁻¹ motion between the Highlands and the Solomon Sea (NGH1) not apparent in seismicity. Motion at the Trobriand trough [*Kirchoff-Stein*, 1992] and the Aure Belt [*Kugler*, 1993] is no more than a few millimeters per year, accounting for a small fraction of the needed slip. The problem is alleviated if the Manus basin velocities are 10-20% too high or if the Huon Peninsula is moving 10-30 mm yr⁻¹ west with respect to the South Bismarck plate, so that the New Guinea Highlands (NGH2) have little movement relative to Australia. The irregular temporal occurrence of large earthquakes (most in the last 30 years occurred in 1970, 1987, and 1992) suggests that additional deformation zones may remain to be discovered.

Conclusions

1. The primary mode of deformation in the Finisterre region appears to be thrust faulting along the RM thrust fault zone, although some large earthquakes indicate strike-slip deformation of the overriding HF block.

2. Thrust earthquakes with dips of 30°-40° are found at 25-35 km depth beneath the north coast of the Huon Peninsula. These events probably represent faulting on a downdip extension of the RM fault system.

3. Movement on these thrust earthquakes may cause the uplift observed in Pleistocene terraces along the north coast of the Huon Peninsula. Uplift rates and the last 93 years of seismicity are consistent with a significant ($M_0 = 10^{19} - 10^{20}$ N m) event sequence every 30-100 years, although larger, less frequent events cannot be ruled out.

4. Gravity observations show a steep negative gradient northward from the RM fault. The gradient and strongly negative values are not predicted by regional or local isostatic compensation of topography and require additional loads or bending moments to depress the crust of the HF mountains. The additional load is comparable to the topographic load of the mountains and produces 2-4 km of deflection across the Markham basin.

5. Four thrust earthquakes show faulting at 20-25 km depth beneath the south coast of the Huon Peninsula, with north dipping nodal planes dipping 5°-20°. These events cannot be easily explained as thrusting on the RM fault system, but instead suggest faulting on deeper thrust systems which surface farther to the south (Figure 8).

6. Large strike-slip faulting sequences show deformation confined to the upper plate of the HF collision. Slip vectors of these events are everywhere perpendicular to the arcuate RM Fault-New Britain Trench strike and may result from along-strike differences in resistance to convergence.

7. Slip vectors in the HF collision zone are consistently rotated 20°-30° clockwise relative to slip vectors at the New Britain trench, with a transition near 148°E. These vectors require either E-W convergence between the Solomon Sea and New Guinea, or E-W extension between the Huon Peninsula and New Britain. The slip vector azimuths are difficult to reconcile with previously published plate motions, suggesting that either some microplate values are in error or additional regions of deformation are present.

Appendix

Waveforms for the six events occurring before 1977 are shown (Figure A1). Complexities of the fitting are discussed below.

Event 661223. Most stations show a compressional first arrival indicating a high-angle thrust mechanism, but stations hkc, shk and mat to the north show impulsive dilatational first arrivals with amplitudes much larger than could be generated with a simple double couple mechanism. The width of the first half cycle was 1-3 s at these stations to the north, as opposed to 6-9 s for the first (compressional) half cycle at other stations. The widths could not be matched as a depth phase but suggests that an earlier subevent preceded the main shock to the three northern stations. Because the only constraints on the earlier subevent are three dilatational first ar-

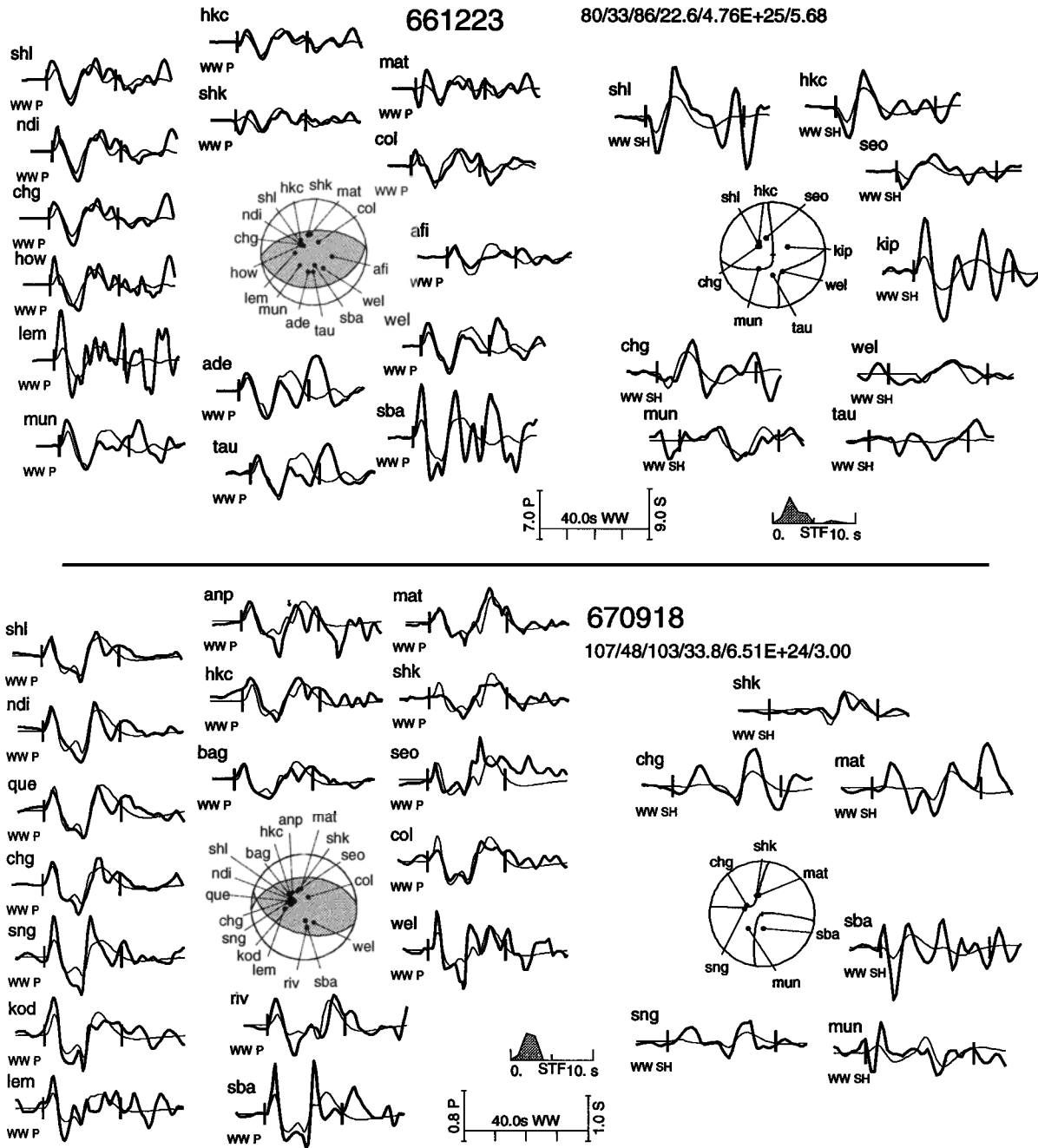


Figure A1. Waveforms and inversion results for all earthquakes from Table 1 not in the Harvard CMT catalog. *P* waveforms shown at left, and *SH* at right, along with nodes of each radiation pattern and locations of rays leaving for each station. Each seismogram is labeled by station code, upper left, and wave type, lower right (WW *P* for analog *P* waves, WW *SH* for analog *SH*). Timescale and amplitude scale are shown for each figure. Amplitudes (in centimeters) are corrected to instrument magnification of 3000 and 40° distance, with separate scales for *P* and *SH*. STF is source-time function at a different timescale. Solution parameters are labeled on each figure, as strike/dip/rake/depth/seismic moment/duration, where angles are in degrees, depth is in kilometers, seismic moment is in dyne centimeters, and duration is 95% duration of STF, in seconds. Other symbols are the same as in Figure 4.

rivals its source parameters are poorly constrained. A single mechanism is presented here, which is consistent with the main parts of the seismograms but violates first motion polarities at the three northern stations.

Event 670918. This moderate-sized thrust event is similar to events in the 1992 sequence.

Madang Earthquake Sequence (701031-720119). The October 31, 1970, Madang earthquake (Figure A1) was one

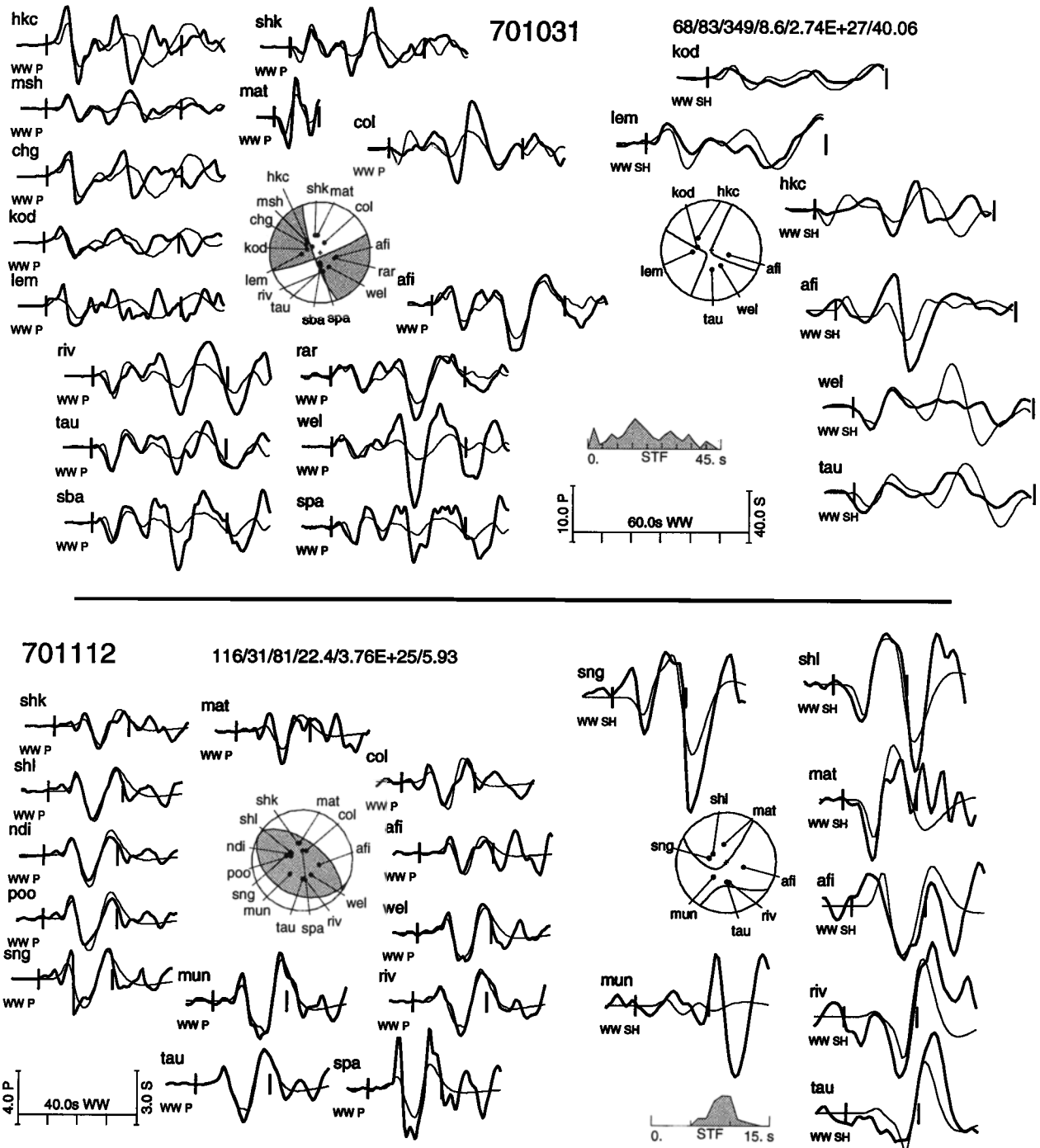


Figure A1. (continued)

of the most damaging recent earthquakes in Papua New Guinea [Everingham, 1975]. Numerous aftershocks recorded by stations in Papua New Guinea show a WSW-ENE trend extending 100 km (Figure 3a) [Everingham, 1975]. The main event indicates primarily left-lateral slip on a WSW-ENE fault plane (subparallel to the aftershock trend), while the largest aftershock, 701112, showed high-angle thrust faulting on a fault plane striking NW-SE.

The mainshock's source time function shows an initial sharp peak and a second peak 20-30 s after the first arrival,

which correspond to two distinct arrivals on most seismograms. Comparison with waveforms for a nearby, smaller strike-slip event (720118) shows that the large, late phases observed to the south are seen only for the mainshock, so probably represent a second source with different orientation. However, for simplicity a single source was assumed. First, the first 20 s of the seismograms were inverted to obtain a fault plane solution consistent with first motions. The entire seismogram was then inverted for moment and source time function, with the nodal planes fixed. The fit to later parts of the

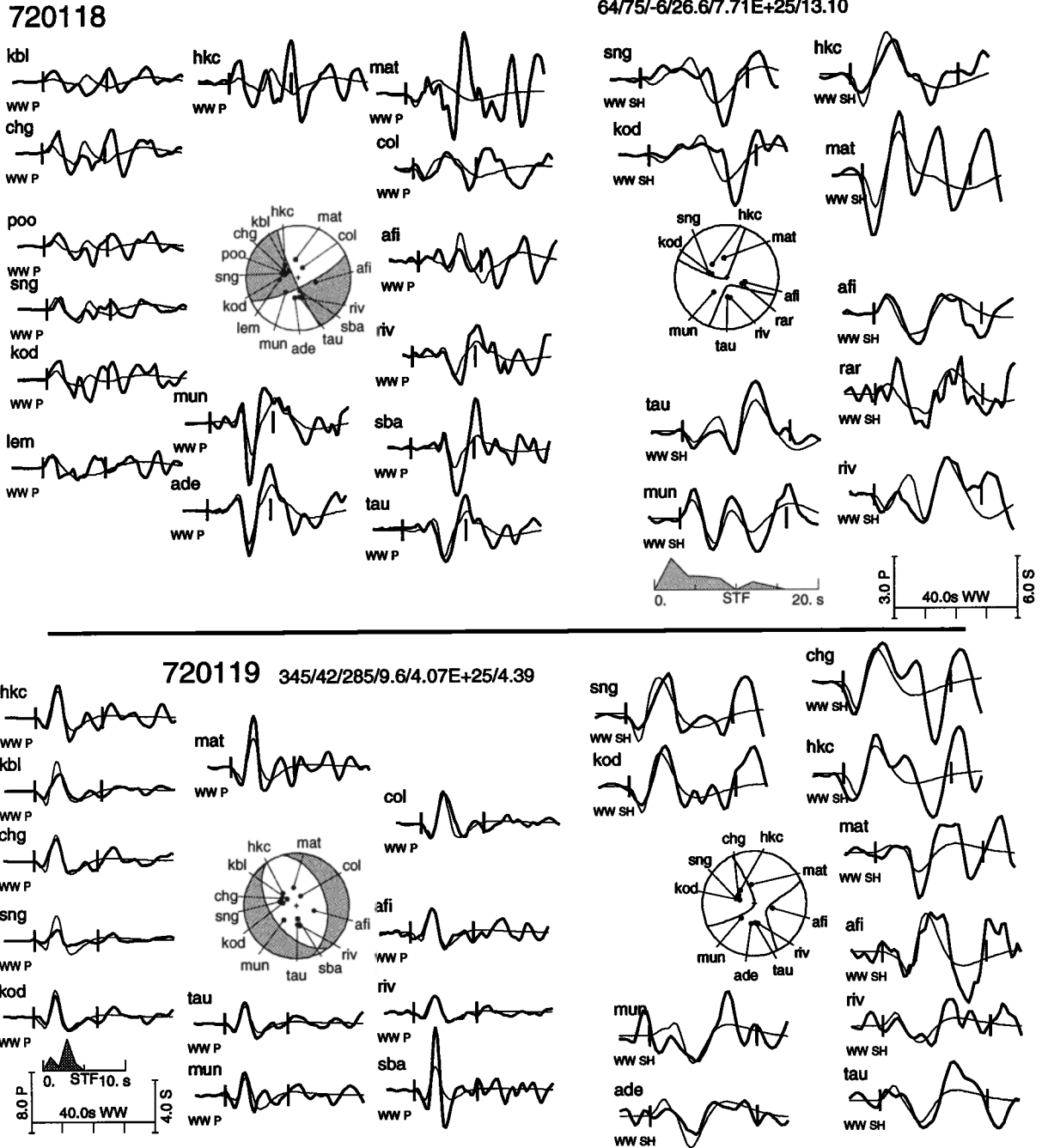


Figure A1. (continued)

waveform was slightly improved (~5% variance reduction) when rupture propagation to the NE was assumed (results listed in Table 2) and was degraded when propagation to the SW was modeled, even though the hypocenter is at the NE end of the aftershock zone. The seismic moment predicts a fault slip of 6 m, assuming a seismogenic layer thickness of 15 km and a fault length of 85 km as indicated by aftershocks.

Note Added In Proof. Shortly after acceptance of this paper, two $M_s > 7.0$ earthquakes and several smaller events occurred near the southern flanks of the Finisterre mountains, 0-30 km north of the Ramu-Markham Valley near 146°E. The largest two events occurred on October 13, 1993 (M_s 7.2) and October 25, 1993 (M_s 7.1) and caused

numerous landslides, loss of life, and other damage. These are the largest events near the RM valley since global seismic recording began. Preliminary analysis suggests these events are similar to most other south Huon events; they show low-angle thrust mechanisms that strike parallel to the RM valley, at depths near 20 km. As with the other south Huon events, these events are too deep to occur on a simple down-dip extension of the RM fault, and show that (1) the deeper fault surface extends west along strike, and (2) the fault is capable of generating significant earthquakes.

Acknowledgments. We thank A. Snow, Z. Sombo, and the UNITECH Surveying Department, Lae, for surveying remote gravity stations. We also thank Chris Kulig for assistance in the field, E. Silver

for use of his gravity meter, R. Rogerson and H. Letz for logistical support, M. Easom for boat transport, and someone named John for leading us to civilization after the boat sank. We thank the IRIS Data Management Center personnel for help with digital waveforms, and M. Yamasaki and D. DeLoatch for running the Lamont film chip library.

We appreciate discussions with E. Silver and L. Abbott, and reviews by H. Davies, R. Page, L. Seeber, and J. Weissel. This research was funded under NSF grants EAR-8608405 and EAR-8720773. Lamont-Doherty contribution number 5159.

References

- Abbott, L.D., and E.A. Silver, Geology of the southern Finisterre range: A case history of modern arc-continent collision, in *Proceedings of the PNG Geology, Exploration, and Mining Conference*, Australas. Inst. Min. and Metall., Parkville, Victoria, Australia, pp. 1-7, 1991.
- Abers, G.A., Active tectonics and seismicity of New Guinea, Ph. D. thesis, Mass. Inst. of Technol., Cambridge, 255 pp., 1989.
- Abers, G., and R. McCaffrey, Active deformation in the New Guinea Fold-and-Thrust Belt: Seismological evidence for strike-slip faulting and basement-involved thrusting, *J. Geophys. Res.*, 93, 13,332-13,354, 1988.
- Abers, G.A., and H. Lyon-Caen, Regional gravity anomalies, depth of the foreland basin, and isostatic compensation of the New Guinea Highlands, *Tectonics*, 9, 1479-1493, 1990.
- Abers, G.A., and S. Roecker, Deep structure of an arc-continent collision: Earthquake relocation and inversion for upper mantle *P* and *S* wave velocities beneath Papua New Guinea, *J. Geophys. Res.*, 96, 6379-6401, 1991.
- Aki, K., and P.G. Richards, *Quantitative Seismology, Theory and Methods*, 557 pp., W.H. Freeman, New York, 1980.
- Brune, J. N., Seismic moment, seismicity, and rate of slip along major fault zones, *J. Geophys. Res.*, 73, 777-784, 1968.
- Bureau of Mineral Resources, Geology and Geophysics (BMR), Gravity Map of Melanesia, Bur. of Min. Res., Canberra, Australia, 1979.
- Chappell, J., Geology of coral terraces, Huon Peninsula, New Guinea: A study of Quaternary tectonic movements and sea-level changes, *Bull. Geol. Soc. Am.*, 85, 553-570, 1974.
- Cook, F.A., D.S. Albaugh, L.D. Brown, S. Kaufman, J.E. Oliver and R.D. Hatcher, Thin-skinned tectonics in the crystalline southern Appalachians; COCORP seismic-reflection profiling of the Blue Ridge and Piedmont, *Geology*, 7, 563-567, 1979.
- Cooper, P., and B. Taylor, Seismotectonics of New Guinea: A model for arc reversal following arc-continent collision, *Tectonics*, 6, 53-67, 1987.
- Crook, K.A.W., Quaternary uplift rates at a plate boundary: implications for seismic risk, Lae urban area, PNG, *IOC WESTPAC Symposium on the Indo-Pacific Convergence Zone, Program and abstracts*, p. 20, Intergovernmental Oceanographic Commission, Paris, 1986.
- Cullen, A. B., and J. D. Pigott, Post-Jurassic tectonic evolution of Papua New Guinea, *Tectonophysics*, 162, 291-302, 1989.
- D'Addario, G. W., D. B. Dow, and R. Swoboda, Geology of Papua New Guinea, scale 1:2 500 000, Bur. Min. Res., Canberra, Australia, 1976.
- Dalmayrac, B., and P. Molnar, Parallel thrust and normal faulting in Peru and constraints on the state of stress, *Earth Planet. Sci. Lett.*, 55, 473-481, 1981.
- Davies, H.L., J. Lock, D.L. Tiffin, E. Honza, Y. Okuda, F. Murakami, and K. Kisimoto, Convergent tectonics in the Huon Peninsula region, Papua New Guinea, *Geo-Mar. Lett.*, 7, 143-152, 1987.
- DeMets, C., R. Gordon, D. Argus, and S. Stein, Current plate motions, *Geophys. J. Int.*, 101, 425-478, 1990.
- Dewey, J. F., and J. M. Bird, Mountain belts and the new global tectonics, *J. Geophys. Res.*, 75, 2625-2647, 1970.
- Dmowska, R., L.C. Lovison-Golob, and J.J. Durek, Partial breaking of a mature seismic gap: The 1987 earthquakes in New Britain, *Pure Appl. Geophys.*, 136, 459-477, 1991.
- Dow, D.B., A geological synthesis of Papua New Guinea, *Bull. Bur. Min. Res. Aust.*, 201, 41 pp., 1977.
- Dziewonski, A.M., T.-A. Chou, and J.H. Woodhouse, Determination of earthquake source parameters from waveform data for studies of global and regional seismicity, *J. Geophys. Res.*, 86, 2825-2852, 1981.
- Ekström, G., A very broad band inversion method for the recovery of earthquake source parameters, *Tectonophysics*, 166, 73-100, 1989.
- Everingham, I. B., Large earthquakes in the New Guinea-Solomon islands area, 1873-1972, *Tectonophysics*, 23, 323-338, 1974.
- Everingham, I. B., Seismological report on the Madang earthquake of 31 October 1970 and aftershocks, *Aust. Bur. Min. Res. Rep.*, 176, 1975.
- Falvey, D.A., and T. Prichard, Preliminary paleomagnetic results from northern Papua New Guinea: Evidence for large microplate rotations, *Trans. Circumpacific Eng. Min. Res. Conf.*, 3, 593-599, 1982.
- Fitch, T. J., Plate convergence, transcurrent faults and internal deformation adjacent to southeast Asia and the western Pacific, *J. Geophys. Res.*, 77, 4432-4460, 1972.
- Hamilton, W., Tectonics of the Indonesian region, *U.S. Geol. Surv. Prof. Pap.*, 1078, 345 pp., 1979.
- Harvey, D., and G.L. Choy, Broadband deconvolution of GDSN data, *Geophys. J. R. Astron. Soc.*, 69, 659-668, 1982.
- Huang, P. Y., S. C. Solomon, E. A. Bergman, and J. L. Nabelek, Focal depths and mechanisms of Mid-Atlantic Ridge earthquakes from body waveform inversion, *J. Geophys. Res.*, 91, 579-598, 1986.
- Jenkins, D. A., Detachment tectonics in western Papua New Guinea, *Bull. Geol. Soc. Am.*, 85, 533-548, 1974.
- Johnson, T., and P. Molnar, Focal mechanisms and plate tectonics of the southwest Pacific, *J. Geophys. Res.*, 77, 5000-5032, 1972.
- King, J., H. Letz, and J. Buleka, Report on the effects of the Vitiaz Strait earthquake of 9th February 1987 Morobe Province, *Geol. Surv. Papua New Guinea Rep.* 87/3, 55 pp., 1987.
- Kirchoff-Stein, K.S., Seismic reflection study of the New Britain and Trobriand subduction systems and their zone of initial contact in the western Solomon Sea, Ph.D. thesis, U.C. Santa Cruz, 1992.
- Krause, D. C., Submarine geology north of New Guinea, *Bull. Geol. Soc. Am.*, 76, 27-42, 1965.
- Kugler, K., Detailed analysis from seismic data of the structure within the Aure Fold and Thrust Belt, Gulf of Papua, Papua New Guinea, in Carman, G.J. and Z., editors, *Petroleum Exploration and Development in Papua New Guinea; Proceedings of the 2nd PNG Petroleum Convention*, Brown Prior Anderson Pty., Australia, pp. 399-411, 1993.
- Kulig, C., R. McCaffrey, G.A. Abers, and H. Letz, Shallow seismicity of arc-continent collision near Lae, Papua New Guinea, *Tectonophysics*, in press, 1994.
- Lyon-Caen, H., and P. Molnar, Constraints on the structure of the Himalaya from an analysis of gravity anomalies and a flexural model of the lithosphere, *J. Geophys. Res.*, 88, 8171-8191, 1983.
- McCaffrey, R., Active tectonics of the eastern Sunda and Banda arcs, *J. Geophys. Res.*, 93, 15,163-15,182, 1988.
- McCaffrey, R., and G.A. Abers, Orogeny in arc-continent collision: The Banda Arc and Western New Guinea, *Geology*, 19, 563-566, 1991.
- McCaffrey, R., G. Abers, and P. Zwick, Inversion of teleseismic body waves, in *Digital Seismogram Analysis and Waveform Inversion, IASPEI Software Library, vol. 3*, edited by W.H.K. Lee, pp. 81-166, Seismol. Soc. Am., El Cerrito, Calif., 1991.
- McKenzie, D., and J. Jackson, The relationship between strain rates, crustal thickening,

- paleomagnetism, finite strain, and fault movements within a deforming zone, *Earth Planet. Sci. Lett.*, **65**, 182-202, 1983.
- Milsom, J.S., Papuan Ultramafic Belt: Gravity anomalies and the emplacement of ophiolites, *Bull. Geol. Soc. Am.*, **84**, 2243-2258, 1973.
- Molnar, P., and D. Gray, Subduction of continental lithosphere: Some constraints and uncertainties, *Geology*, **7**, 58-62, 1979.
- Mori, J., C. McKee, and H. Letz, The Central New Britain earthquake of May 10, 1985: tensional stresses in the frontal arc, *Phys. Earth Planet. Int.*, **48**, 73-78, 1987.
- Nábělek, J., Determination of earthquake source parameters from inversion of body waves, Ph.D. thesis, 262 pp., Mass. Inst. of Technol., Cambridge, 1984.
- Nábělek, J., Geometry and mechanism of faulting of the 1980 El Asnam, Algeria, earthquake from inversion of teleseismic body waves and comparison with field observations, *J. Geophys. Res.*, **90**, 12,713-12,728, 1985.
- Pettifer, G.R., Markham valley gravity survey Papua New Guinea 1972, *Aust. Bur. Min. Res. Geol. Geophys. Rec.*, **1974/65**, 9 pp., 1974.
- Plafker, G., W.J. Nokleberg, and J.S. Lull, Bedrock geology and tectonic evolution of the Wrangellia, Peninsular, and Chugach terranes along the Trans-Alaska Crustal Transect in the Chugach mountains and southern Copper River basin, Alaska, *J. Geophys. Res.*, **94**, 4255-4296, 1989.
- Robinson, G.P., Huon-Sag Sag, Papua New Guinea, scale 1:250 000, Geol. Ser. Explan. Notes, Geol. Surv. Papua New Guinea, 1974.
- Rogerson, R., D. Hilyard, and E. Silver, Excursion guide to the Papua New Guinea collision zone, *Geol. Surv. Papua New Guinea Rep.* **88/17**, 98 pp., 1988.
- Silver, E.A., D.L. Reed, J. Galewsky, and L.D. Abbott, Synthesis of HAWAII MR1 and seismic study of the western Solomon sea collision zone, *EOS Trans. AGU*, **73**, 535, 1992.
- Silver, E.A., L.D. Abbott, K.S. Kirchoff-Stein, D.L. Reed, and B. Bernstein-Taylor, Collision propagation in Papua New Guinea and the Solomon Sea, *Tectonics*, **10**, 863-874, 1991.
- Simpson, D. W., R. F. Mereu, and D. W. King, An array study of P-wave velocities in the upper mantle transition zone beneath north-eastern Australia, *Bull. Seismol. Soc. Am.*, **64**, 1757-1788, 1974.
- St. John, V.P., The gravity field in New Guinea, Ph.D. thesis, 347 pp., Univ. of Tasmania, Hobart, 1967.
- St. John, V.P., The gravity field and structure of Papua and New Guinea, *APEA J.*, **10**, 41-55, 1970.
- Stein, S., and D. Wiens, Depth determination for teleseismic earthquakes: Methods and results, *Rev. Geophys.*, **24**, 806-832, 1986.
- Talwani, M., J.L. Worzel and M. Landisman, Rapid gravity computations for two-dimensional bodies with application to the Mendocino submarine fracture zones, *J. Geophys. Res.*, **64**, 49-59, 1959.
- Taylor, B., Bismarck Sea: Evolution of a back-arc basin, *Geology*, **7**, 171-174, 1979.
- Telford, W.M., L.P. Geldard, R.E. Sheriff, and D.A. Keys, *Applied Geophysics*, 860 pp., Cambridge University Press, New York, 1976.
- von der Borch, C.C., Marine geology of the Huon Gulf region, New Guinea, *Bull. Bur. Miner. Resour. Geol. Geophys. (Aust.)*, **127**, 36pp., 1972.
- Weissel, J. K., and R. N. Anderson, Is there a Caroline Plate?, *Earth Planet. Sci. Lett.*, **41**, 143-158, 1978.
- Weissel, J. K., B. Taylor, and G. D. Karner, The opening of the Woodlark Basin, subduction of the Woodlark spreading system, and the evolution of northern Melanesia since mid-Pliocene time, *Tectonophysics*, **87**, 253-277, 1982.
- Wellman, P., Yu. D. Boulanger, B.C. Barlow, S.N. Shcheglov, and D.A. Coutts, Australian and Soviet gravity surveys along the Australian calibration line, *Bull. Bur. Miner. Resour. Geol. Geophys. (Aust.)*, **161**, 172 pp., 1974.
- Woollard, G.P., The new gravity system — Changes in international gravity base values and anomaly values, *Geophysics*, **44**, 1352-1366, 1979.
- Zhang, J., and T. Lay, A new method for determining the long-period component of the source time function of large earthquakes, *Geophys. Res. Lett.*, **16**, 275-278, 1989.

G. A. Abers, Lamont-Doherty Earth Observatory, Route 9W, Palisades, N.Y. 10964. (e-mail: abers@ldeo.columbia.edu)

R. McCaffrey, Rensselaer Polytechnic Institute, Department of Earth and Environmental Science, Troy, N.Y., 12180.

(Received May 3, 1993; revised October 15, 1993; accepted October 21, 1993.)